Functional analysis across model systems implicates ribosomal proteins in growth and proliferation defects associated with hypoplastic left heart syndrome

Tanja Nielsen[1,6,*], Anaïs Kervadec[1,*], Jeanne L. Theis[2,*], Maria A. Missinato[1], James Marchant[1], Michaela Romero[1], Katya Marchetti[1], Aashna Lamba[1], Xin-Xin I. Zeng[1], Marie Berenguer[1], Stanley M. Walls[1], Analyne Schroeder[1], Katja Birker[1], Greg Duester[1], Paul Grossfeld[5], Timothy J. Nelson[3], Timothy M. Olson[4,], Karen Ocorr[1], Rolf Bodmer[1,#], Georg Vogler[1,#], Alexandre R. Colas[1,#]

[1] Center for Cardiovascular and Muscular Diseases, Sanford Burnham Prebys Medical Discovery Institute, 10901 North Torrey Pines Road, La Jolla, CA, 92037, USA

[2] Cardiovascular Genetics Research Laboratory, Mayo Clinic, Rochester, MN, USA

[3] Center for Regenerative Medicine, Division of Pediatric Cardiology, Department of Pediatric and Adolescent Medicine, Division of General Internal Medicine, Department of Molecular and Pharmacology and Experimental Therapeutics, Mayo Clinic, Rochester, MN, USA

[4] Department of Cardiovascular Medicine, Division of Pediatric Cardiology, Department of Pediatric & Adolescent Medicine, Cardiovascular Genetics Research Laboratory, Mayo Clinic, Rochester, MN, USA

[5] University of California San Diego, Rady Children's Hospital, San Diego, CA, USA.

[6] Department of Biochemistry, Chemistry and Pharmacy, Freie Universität Berlin, Berlin, Germany

* These authors contributed equally

[#] Co-corresponding authors

Keywords: Congenital heart disease, HLHS, whole genome sequencing, rare variant filtering, cardiogenesis, *Drosophila*, iPSC, zebrafish, *RPS15A*, *TP53*, *yorkie*, *tinman/NKX2-5, Dorsocross/TBX5*, *pannier/GATA6*.

Abstract

Hypoplastic left heart syndrome (HLHS) is the most lethal congenital heart disease (CHD). The pathogenesis of HLHS is poorly understood, and due to the likely oligogenic complexity of the disease, definitive HLHS-causing genes have not yet been identified. Postulating impaired cardiomyocyte proliferation as a likely important contributing mechanism to HLHS pathogenesis, and we conducted a genome-wide siRNA screen to identify genes affecting proliferation of human iPSC-derived cardiomyocytes (hPSC-CMs). This yielded ribosomal protein (RP) genes as the most prominent class of effectors of CM proliferation. In parallel, whole genome sequencing and rare variant filtering of a cohort of 25 HLHS proband-parent trios with poor clinical outcome revealed enrichment of rare variants of RP genes. In addition, in a familial CHD case we identified a rare, predicted-damaging promoter variant affecting *RPS15A* that was shared between the HLHS proband and a distant relative with CHD. Functional testing with an integrated multi-model system approach reinforced the idea that RP genes are major regulators of cardiac growth and proliferation, thus potentially contributing to the hypoplastic phenotype observed in HLHS patients. Cardiac knockdown (KD) of RP genes with promoter or coding variants (*RPS15A, RPS17, RPL26L1, RPL39, RPS15*) reduced proliferation in generic hPSC-CMs and caused malformed hearts, heart-loss or even lethality in *Drosophila*. In zebrafish, diminished *rps15a* function caused reduced CM numbers, heart looping defects, or weakened contractility, while reduced *rps17* or *rpl39* function caused reduced ventricular size or systolic atrial dysfunction of the atrium, respectively. Importantly, genetic interactions between *RPS15A* and core cardiac transcription factors *TBX5* in CMs, *Drosocross, pannier* and *tinman* in flies, and *tbx5* and *nkx2-7* (*nkx2-5* paralog) in fish, support a specific role for RP genes in heart development. Furthermore, *RPS15A* KD-induced heart/CM proliferation defects were significantly attenuated by *p53* KD in both hPSC-CMs and zebrafish, and by Hippo activation (*YAP/yorkie* overexpression) in developing fly hearts. Based on these findings, we conclude that RP genes play novel critical roles in cardiogenesis and constitute an emerging class of gene candidates likely involved in HLHS.

64 **Introduction**

65 Hypoplastic left heart syndrome (HLHS) accounts for 2-3% of all cases of
66 congenital heart disease (CHD) [1, 2] and is characterized by underdevelopment of the
67 left ventricle, mitral and aortic valves, and aortic arch [3]. HLHS has a recognized genetic
68 component based on its familial association with left-sided obstructive congenital heart
69 diseases [4-6]. However, segregation analyses in multiplex HLHS-CHD families [6] and
70 genome-wide association studies (GWAS) of large cohorts [5] have lacked sufficient
71 power to conclusively identify candidate HLHS-susceptibility genes with small to
72 moderate effect sizes. Defects in a small number of genes involved in cardiogenesis,
73 such as *NOTCH1* [7], *NKX2–5* [8], *MYH6* [9], and *GATA4* [8, 10] have been implicated
74 as contributors to HLHS, as well as multiple other CHDs. However, the variety of
75 phenotypic manifestations of HLHS, together with numerous studies linking it to diverse
76 genetic loci [7-9, 11], suggests that HLHS is genetically heterogeneous and has a
77 multigenic etiology [12, 13].

78 It has also been hypothesized that the underdevelopment of the left ventricular
79 myocardium includes restricted blood flow across the mitral valve and its hemodynamic
80 effect during ventricular growth and development ("no flow – no grow" [14]), as well as
81 endocardial defects [15]. Therefore, HLHS manifestation may be due to a combination of
82 cardiomyocyte autonomous and non-autonomous genetic as well as mechanical effects,
83 all of which likely affect proliferation and differentiation in the developing heart.

84 In a digenic HLHS mouse model, loss of both Sin3A Associated Protein 130
85 (*Sap130)* and the protocadherin *Pcdha9* cause decreased CM proliferation resulting in
86 left ventricular (LV) hypoplasia [16]. In addition, LVs from HLHS patients have cardiac
87 damage associated with CM proliferation defects compared to healthy subjects [17].
88 These studies suggest that intrinsically defective cardiac differentiation and impaired CM
89 proliferation are likely contributing to HLHS-associated heart defects. Further
90 strengthening this hypothesis, we found that HLHS-patient-derived hPSC-CMs exhibited
91 reduced proliferation compared to the parents [18]. There is a need to identify the
92 potentially causative genes, which contribute to those processes described above and to
93 elucidate their role HLHS pathogenesis.

94 To advance CHD gene discovery, we have developed a multi-model systems
95 platform enabling to both rigorously prioritize candidate genes from whole-genome
96 sequencing (WGS) based on rare, predicted-damaging variants and their mode of
97 inheritance, and to functionally characterize gene function in complementary and
98 genetically tractable model systems: human induced pluripotent stem cells (hPSC), the
99 fruit fly *Drosophila melanogaster* and zebrafish *Danio rerio*. The genetic basis of cardiac
100 development, originally uncovered in *Drosophila*, is fundamentally conserved across
101 species [19-22] and ~80% of human disease genes have fly orthologs [23]. In addition,
102 the non-redundant fly genome together with the simple structure and function of the fly
103 heart allow straightforward genotype-phenotype correlations. Zebrafish [24-26], which
104 has a two-chambered heart and can be easily manipulated using morpholino injections
105 and CRISPR technologies to affect heart development and function. In addition,
106 phenotypes can be directly observed in the developing larva for several days post
107 fertilization [27]. Finally, cardiomyocytes (CMs) differentiated from hPSCs (hPSC-CMs)
108 enable to identify and quantify cellular phenotypes associated with human diseases,
109 including HLHS [7, 28-30] and are amenable to large scale functional screens [31, 32],
110 thereby enabling to serve both as a discovery and validation platform. This integrated
111 approach allows to rapidly identify novel HLHS-associated gene candidates and to
112 characterize their ability to regulate developmental processes associated with disease
113 (e.g., hypoplasia) [18].

114 Defective CM proliferation is likely a hallmark of HLHS [16-18], thus to uncover
115 novel regulators of human CM proliferation with potential links to HLHS, we performed a
116 whole genome siRNA screen (18,055 genes) using an EdU assay in hPSC-CMs and
117 identified ribosomal proteins (RPs) as the major class of genes controlling CM
118 proliferation. In parallel, whole genome sequencing (WGS) of 25 poor-outcome HLHS
119 proband-parent trios followed by unbiased variant filtering, revealed an enrichment for
120 rare, predicted-damaging variants in RP genes. Moreover, analysis of a high-value family
121 (75H) comprised of a HLHS proband, his phenotypically normal parents, and a fifth
122 degree relative born with left-sided CHD led to the identification of a predicted-damaging
123 variant in RP protein gene *RPS15A* that segregated with disease. Consistent with a
124 central role for RPs in the regulation of heart development, heart-specific knock-down

125 (KD) of HLHS-associated RPs in *Drosophila* caused severe phenotypes, including near
126 complete heart-loss and lethality. Similarly, in zebrafish, *rps15a* CRISPR mutants and
127 morphants had greatly reduced heart size and CM number, looping defects and
128 diminished contractility. In this context, a multi-model system evaluation (hPSC-CMs, flies
129 and zebrafish) of RP function show their important role on heart growth and differentiation
130 and CM proliferation by modulating the p53, Myc and Hippo pathways. Moreover, we find
131 evidence that RPs may regulate heart development and CM proliferation in a cardiac-
132 specific manner by synergistically interacting with core cardiac transcription factors such
133 as T-box, Nkx and Gata factors. In sum, here we show that RP genes are potent
134 regulators of CM proliferation and cardiac growth and differentiation, consistent with a
135 potentially critical role in the hypoplastic phenotype of HLHS. We suggest that RP genes
136 are an emerging class of novel genetic effectors in HLHS.

137 **Results**

138

139 **Whole genome siRNA screen identifies ribosomal proteins as central regulators of**
140 **cardiomyocyte proliferation**

141 Based on previous and our recent data [16-18], impaired CM proliferation is
142 emerging as an important mechanism in HLHS pathogenesis. Thus, to comprehensively
143 map the human genome for novel regulators of CM proliferation, we screened a library of
144 18,055 siRNAs for their ability to modulate proliferation in human iPSC-derived CMs
145 (hPSC-CMs). To assess CM proliferation, we used a dual read-out and quantified both
146 DNA synthesis using EdU incorporation [31], and total number of CMs, 3 days after
147 treatment (**Figure 1A-C**). Briefly, siRNAs were transfected into 25-day old hPSC-CMs
148 [29, 33]. After 2 days, EdU was added to the wells for 24 hours. On day 3, cells were fixed
149 and co-stained for sarcomeric protein alpha-Actinin (ACTN2), EdU, and DAPI. Next, the
150 number of EdU/alpha-Actinin double-positive cells, and the total number of CMs were
151 determined using a commercially available high-throughput image analysis software
152 (MetaXpress, Molecular Devices)[31]. Note that alpha-Actinin-, EdU+ cells which typically
153 express fibroblast markers (i.e POSTN)[34], were excluded from this analysis, to focus
154 on CM biology only. In total, we found 153 siRNAs that decreased proliferation (< 0.5-fold
155 EdU incorporation) and number of CMs (<0.8-fold), and 162 siRNAs that increased EdU
156 (>1.2-fold) and CM number (>1.1-fold; **Figure 1B, C and Supplemental Table 1 WGS**
157 **data**). Consistent with previous studies [35, 36], KD of cell cycle checkpoint agonist,
158 CHEK1 and MDM2, the negative regulator of TP53, both were among top hits that
159 reduced CM proliferation. As expected, we identified TP53 and CDKN1A among the
160 genes that significantly increased CM cell number upon KD (**Figure 1B, C**). Next, to gain
161 insight into the molecular pathways regulating proliferation in hPSC-CMs, we performed
162 Gene Ontology (GO) term analysis of hits decreasing EdU incorporation or CM numbers
163 and found an enrichment for genes associated with “translation/ribosome” and p53
164 signaling as top hits (**Figure 1D, E**). Consistent with these observations, we had
165 previously found that the p53 pathway is dysregulated in hPSCs differentiated from a
166 HLHS family trio [18]. Remarkably, the most represented gene family are ribosomal
167 proteins (RPs), KD of which caused consistently the strongest inhibition of cell

168 proliferation (**Figure 1B**). Next, since, the primary screen was performed as a single data
169 point, we next sought to validate these findings by re-testing all 80 RP genes for function
170 [37] using a distinct set of siRNAs in biological quadruplicate conditions. Remarkably and
171 consistent with the primary screen, KD of 59/80 RPs significantly reduced proliferation as
172 compared to siControl ($p<0.05$; **Supplemental Figure 1A, B**). In this context, further
173 functional testing in fibroblasts revealed that the antiproliferative effect of RP loss of
174 function is cell type–independent (**Supplemental Figure 1C, D)**. Together, these findings
175 establish RP function as essential for cell proliferation, including in hPSC-CMs, and
176 suggest that RPs may represent a previously unrecognized class of regulators of
177 ventricular growth during embryonic development.
178

179 **Enrichment of RP gene variants in an HLHS patient cohort with poor clinical**
180 **outcome**

181 To identify candidate genes involved in HLHS pathogenesis, we performed whole
182 genome sequencing (WGS), variant filtering, and enrichment analysis (see also [18], and
183 Methods: WGS and bioinformatic strategies) in a cohort of 25 HLHS patient-parent trios
184 with poor clinical outcome defined as either prenatal – restrictive atrial septal defect (n=2);
185 postnatal – reduced right ventricular ejection fraction following stage II or III surgical
186 palliation (n=19); protein-losing enteropathy (n=2); or cardiac transplantation/failed
187 surgical palliation (n=2). The 25 probands were comprised of 18 males and 7 females, 24
188 of whom were of white ancestry. The HLHS phenotype with respect to valve morphology
189 (mitral atresia, MA; mitral stenosis, MS; aortic atresia, AA; aortic stenosis, AS) was:
190 MA/AA in 10, MS/AS in 9, MA/AA in 4, MA/AS in 1 and unknown in 1. CHD in the parents
191 was excluded by echocardiography in all but two families, in which a bicuspid aortic valve
192 was present in the mother. Genomic sequences were filtered for uncommon (MAF < 1%)
193 *de novo* and recessive variants in coding and regulatory regions of genes expressed in
194 the developing heart and predicted to alter protein structure or expression, yielding 292
195 unique HLHS candidate genes that primarily fit a recessive mode of inheritance (Figure
196 **2A and Supplemental Table 2**). To determine whether certain gene networks were over-
197 represented among these variants, we used two online bioinformatics tools (STRING and
198 PANTHER [38, 39]). After applying Fisher's exact test and false discovery rate

199 corrections, RPs were the most enriched class of proteins when compared to the
200 reference proteome, which includes data annotated by protein class (5.24-fold,
201 p=0.0028), and cellular component (7.27-fold, p=0.011). In total, 14 variants found in 9
202 RP genes among 6 HLHS probands were identified, most fitting a recessive inheritance
203 disease model (**Table 1**). These RP variants encompass mutations in upstream promoter
204 regions that potentially affect transcription factor binding sites, as well as non-
205 synonymous substitutions inside the protein coding regions.

206 Next, all 292 prioritized candidate genes were systematically evaluated for effects
207 on the proliferation of hPSC-CMs *in vitro* and for cardiac differentiation of fly hearts *in*
208 *vivo.* Again, loss of RP function (*RPL39, RPL26L1, RPS15, RPS17, RSPS28*) caused the
209 most severe phenotypes on proliferation in hPSC-CMs (**Figure 2B, Supplemental Table**
210 **3**), which was consistent with our genome-wide proliferation screen (see **Figure 1B**). In
211 the fly, KD of RPs in the cardiac lineage and throughout embryonic development was
212 achieved using a *Hand*$^{4.2}$-Gal4 driver (see [40] and methods) and led to partial or
213 complete heart loss (*RpL26, RpL36A, RpL3*) or caused lethality (*RpS17, RpL39, RpS15,*
214 *RpL26, RpL36A*) (Figure **2C**). Also, KD of *RpL10* gave rise to severely constricted hearts,
215 while KD of *RpS28b* caused inflow tract defects (**Figure 2C**). Finally, functional testing of
216 RPs in zebrafish embryos revealed that KD of *rpl39* leads to reduced ventricle size,
217 whereas *rps17* CRISPR mutants exhibit systolic dysfunction (**Figure 2D, E**). In sum, our
218 patient centric approach (cohort of 25 probands) identifies RPs as the most enriched gene
219 category affected by HLHS-associated variants (STRING, PANTHER analysis). In this
220 context, systematic testing in multi-model systems (fly, zebrafish, hPSC-CMs) identifies
221 RPs as most potent regulators of cardiac differentiation, proliferation and contractility
222 among HLHS-associated genes. Collectively, these findings highlight that RPs regulate
223 critical steps of cardiogenesis that are also found to be defective in HLHS probands [41,
224 42] and thus suggest a potential link between RP biology and HLHS phenotypic etiology.
225

226 **RPS15A variant associated with HLHS in familial CHD**

227 To further establish a phenotypic link between RP function and HLHs associated
228 phenotypes, we selected a rare familial CHD case (75H) (**Supplemental Figure 2A**), that

229 is comprised of a young teenager with HLHS (MS/AS) and normal ventricular function
230 following Fontan operation, his phenotypically normal parents, and a 5th degree female
231 relative born with left-sided CHD (bicuspid aortic valve and coarctation of the aorta).
232 Based on these observations, we hypothesized the presence of a heterozygous driver
233 variant exhibiting incomplete penetrance and variable expression. To investigate further,
234 we filtered whole-genome sequencing (WGS) data for rare, predicted-damaging variants
235 in coding and regulatory regions. This analysis identified six prioritized variants
236 (**Supplemental Table 4**), including one located in the *RPS15A* gene locus, shared by the
237 HLHS proband, the unaffected mother, and the proband's fifth-degree relative with
238 congenital heart disease (CHD).
239 We next investigated whether family members carrying these variants (the mother
240 and proband) exhibit defects in cardiomyocyte (CM) proliferation compared to the father.
241 Notably, analysis of EdU incorporation in CMs from the parent-proband trio revealed
242 significantly reduced proliferation in both the proband and mother compared to the father.
243 However, the proband displayed a markedly more severe phenotype than the mother
244 (**Figure 3 A,B)**. Interestingly, this reduction in proliferation appeared to be specific to
245 cardiomyocytes (CMs), as EdU incorporation in the non-CM cell population showed no
246 significant differences among the family members (**Supplemental Fig. 2B**). Collectively,
247 these findings suggest a phenotypic association between the presence of the variants
248 and impaired CM proliferation.
249 Finally, to determine the potential relative contribution of the six genes harboring
250 rare and damaging variants in the regulation of CM proliferation, we performed functional
251 KD experiments in hPSC-CMs *in vitro*. Remarkably, while KD of 5 of the other prioritized
252 genes from the 75H family also resulted in moderate reduced CM proliferation, RPS15A
253 KD produced the most pronounced effect, with over an 85% reduction in proliferation,
254 emerging as the top candidate (**Figure 3C, D**). Together, these findings indicate that
255 RPS15A plays a critical role in regulating cardiomyocyte (CM) proliferation in human
256 pluripotent stem cells (hPSCs) and may influence heart developmental processes that
257 are disrupted in HLHS.
258

259 **RPS15A KD in *Drosophila* and zebrafish causes severe cardiac proliferation and**
260 **differentiation defects**

261 To characterize the role of *RPS15A* during heart development, we first induced a
262 heart-specific KD of *RpS15Aa* in flies (see methods), which caused a partial or complete
263 loss of the heart (**Figure 3E,F**). Note that this phenotype is consistent with our results
264 above and a previous study involving another RP gene (*RPL13*) [43].
265 Next, to evaluate the role of *RP* genes during heart development, we knocked-out *rps15a*
266 in zebrafish (*Danio rerio*) using CRISPR [24-26]. We examined F_0 larva at 72 hpf (hours
267 post fertilization) using high speed digital imaging (SOHA [44], see also methods) and
268 confocal microscopy to monitor heart size and cardiomyocyte numbers respectively.
269 Remarkably, *rps15a* mutant hearts were smaller in size (**Supplemental Fig. 2C,D**), with
270 reduced CM numbers (**Figure 3G,H**). We observed similar effects in response to injection
271 of a *rps15a* morpholino (MO) compared to uninjected larva [45, 46] (**Supplemental**
272 **Figure 3 C,D**). In this context, we also noted that the overall body plan and morphology
273 of *rps15a* CRISPR mutants or morphants were largely unaffected, except for a mild
274 pericardial edema, a possible indicator of heart dysfunction (**Figure 3H**) [47].

275 We quantified cardiomyocyte (CM) number using nuclear markers in Tg(*myl7*:*eGFP*);
276 Tg(*myl7*:*H2A-mCherry*) embryos 72 hpf. CM numbers were predominantly reduced in the
277 ventricle compared to the atrium (**Figure 3G,H)**. We also assessed total cardiac cell
278 numbers and cardiac cell proliferation by phospho-histone H3 (PH3) immunostaining and
279 DAPI to quantify total cardiac cells. We again found that the total cell numbers were
280 significantly reduced in both rps15a morphants and crispants (**Supplemental Figure 4A-**
281 **C**). Importantly, the proportion of proliferating (PH3+) cardiac cells was also decreased in
282 rps15a morphants and crispants at both 24 and 48 hpf, but not at 72 hpf when proliferation
283 normally declines (**Supplemental Fig. 4C**). Collectively, these data support the
284 hypothesis that *RPS15A* is required for CM proliferation and heart morphogenesis (hPSC-
285 CMs, fly and zebrafish), thus suggesting a potential role for RPs as genetic drivers of
286 hypoplasticity observed in HLHS.

287

288 **Ribosomal proteins control CM cell cycle by regulating TP53 pathway activity**

289 To investigate how RPs regulate cell cycle activity in hPSC-CMs, we performed
290 RNA-seq upon KD of *RPS15A* and *RPL39*, which belong to the small and the large
291 ribosomal subunits that harbor predicted-damaging variants in 75H and 151H probands,
292 respectively. Comparison of differential gene expression between *siRPS15A* and
293 *siRPL39* KD revealed that ~53% of genes were commonly dysregulated (**Figure 4A**),
294 indicating the existence of a conserved RP-dependent transcriptional network. Consistent
295 with a central role for RPs in the regulation of proliferation, GO term analysis for
296 differentially expressed genes revealed an enrichment for genes involved in DNA
297 replication, mitosis and DNA damage response mediated by p53, and included the
298 downregulation of positive regulators of cell cycle such as *CDK1*, *CCNA2, AURKA, PCNA*
299 and the upregulation of cell cycle arrest mediators such as *CDKN1A, BTG2, GADD45A*
300 (**Figure 4B** and **Supplemental Tables 5,6**). To confirm these findings, we performed
301 immunostaining for canonical p53 downstream transcriptional target [48], *CDKN1A,* and
302 observed that the percentage of CDKN1A+ CMs was increased by ~60% in response to
303 *RPS15A* KD (**Figure 4C, D**), indicating that RP KD induces cell cycle arrest *via* the
304 activation of the p53 signaling pathway in hPSC-CMs.

305 Next, to evaluate if the reduction in proliferation caused by RP KD is mediated by
306 the p53 signaling pathway in CMs, we co-KD *TP53* or *CDKN1A* along with *RPS15A*, and
307 observed a significant rescue of CM proliferation by EdU incorporation and CM number
308 in comparison to RPS15A KD (**Figure 4E, F** and **Supplemental Figure 4D, E**).

309 Next, we tested if RP-mediated defects in zebrafish can also be rescued by
310 inhibition of p53. To this aim, we used morpholinos to co-KD *p53* with *rps15a* [49] and
311 examined larval hearts at 72 hpf. *p53* MO-mediated KD on its own had little effect on
312 heart function but partially reversed the *rps15a* MO-mediated reduction in heart size and
313 cardiomyocyte numbers (**Figure 4G, H**). Moreover, bradycardia, heart looping and
314 reduced contractility phenotypes of *rps15a* morphants were also rescued by co-KD of *p53*
315 (**Supplemental Figure 4F, G)**. Collectively, these observations support our hypothesis
316 that RPs control cardiac development, including heart size and function, *via* a p53
317 pathway-mediated regulation of CM proliferation.

318

319 **Heart loss in *Drosophila* by RpS15Aa KD is partially rescued by Hippo pathway**
320 **activation**

321 The fly heart develops similarly to the vertebrate heart at early stages [20] and a
322 link between RPs and cell cycle-regulating pathways, such as p53 and Hippo pathways
323 [50], has been proposed to be conserved between mammals and flies [51]. To test
324 whether p53 has a function in fly heart development similar to hPSC-CMs and zebrafish,
325 we performed cardiac co-KD of *RpS15Aa* and *p53* and examined heart structure and
326 function. Co-KD did not rescue the cardiac defects of *RpS15Aa* KD suggesting that *p53*
327 has a different role in flies, as compared to vertebrates, as has been reported previously
328 [52].

329 In vertebrates, TP53 is known to act through the negative regulation of the Hippo
330 pathway [53]. In this context, YAP, a downstream effector of Hippo, has been shown to
331 promote CM proliferation in the mouse heart [54]. We therefore tested if YAP/yorkie can
332 substitute the function of p53 in the fly heart and found that overexpressing the Hippo
333 pathway gene *yorkie* (*yki*), the fly ortholog of YAP, in the developing heart considerably
334 restored *RpS15Aa* KD-induced heart loss in *Drosophila* (**Figure 5A',B**). We also observe
335 formation of adult ostial structures, which indicates that the larval heart underwent partial
336 remodeling to an adult heart during metamorphosis. Further, we found that *yki*-mediated
337 rescue depends on the transcriptional co-factor encoded by *scalloped* (*sd*, *Drosophila*
338 *TEAD1/2/3/4*), since upon *sd* KD, *yki* OE can no longer rescue the *RpS15Aa* KD-induced
339 heart loss (**Figure 5A", B**). Moreover, KD of *sd* in an *RpS15Aa* KD background (without
340 *yki* OE) worsens the *RpS15Aa* KD phenotype (**Figure 5A", B**).

341

342 ***RPS15A* genetically interacts with cardiac transcription factors *nkx2.7*/*tinman,* and**
343 **TBX5/*tbx5a/Dorsocross*, *nkx2.7*/*tinman,* and *Gata4,5,6/pannier* in model systems**

344 The profound importance of RPs for cell growth and proliferation in most cell types
345 ([55] and **Supplemental Figure 1**), raises the question of how tissue specific phenotypes
346 such as those observed in HLHS can arise from the defective function of ubiquitously
347 expressed genes. To address this apparent paradox, we hypothesized that RPs might
348 functionally interact with tissue-specific proteins such as cardiac transcription factors

349 (cTFs), to control CM proliferation. Analysis of the impact of cTFs alone on hPSC-CM
350 proliferation from our whole genome screen, revealed that KD of most cTFs did not cause
351 major proliferation defects (except for e.g., *HES4* and *HOPX*; **Figure 6A**). Among the
352 cTFs, TBX5 is specifically expressed in the left ventricle at stages of intense CM
353 proliferation [56] and thus we next asked if *TBX5* could functionally interact with RPs.
354 Remarkably, while hPSC-CM proliferation was not affected by increasing doses of siTBX5
355 (0-2nM), increasing si*TBX5* dosage in siRP backgrounds led to proportional decrease in
356 EdU incorporation (Two-way ANOVA; **Figure 6B and Supplemental Figure 5A,B**),
357 thereby indicating that *RPs* and *TBX5* genetically interact to regulate proliferation in
358 hPSC-CMs.

359 Conservation of genetic interactions between human and fly cardiac transcription
360 factors and constitutive genes have been identified before [57]. We therefore specifically
361 tested for genetic interaction between *RpS15Aa* and the cardiac TFs *tinman/NKX2-5,*
362 *pannier/GATA4/5/6* and *Dorsocross/TBX5* in adult *Drosophila* hearts. A heterozygous
363 deficiency covering *RpS15Aa* causes moderate dilation of hearts compared to controls
364 (**Supplemental Figure 5C)**. However, when *RpS15Aa* was placed *in trans* to loss of
365 function alleles of cardiac TFs *tinman, pannier* or *Dorsocross1/2/3*, these hearts exhibited
366 significantly deformed hearts, which is only rarely observed in the single heterozygotes
367 (Figure **5C, D**). In addition, *RpS15Aa* heterozygous flies showed a prolonged heart period
368 when combined with a *tinman* or *pannier* heterozygous mutations (**Supplemental Figure**
369 **5C**).

370 Next, we tested whether similar genetic interactions are conserved in zebrafish.
371 Zebrafish expresses the NKX2-5 ortholog *nkx2.7* in the heart and functional studies have
372 shown that both *nkx2.5* and *nkx2.7* play critical roles in cardiac development [58]. To
373 determine whether *rps15a* and *nkx2.7 or tbx5a* genetically interact in zebrafish, we
374 injected low doses of *rps15a* [45] MO, in combination with *nkx2.7* [59] or *tbx5a* MO.
375 *nkx2.7* MO alone had little effect on heart size, cross-sectional area, or contractility,
376 whereas double morphants exhibited cardiac dysfunction, with contraction virtually
377 abolished in some animals (**Supplemental Figure 5D**). Furthermore, we observed a
378 significant prolongation of the heart period in double morphants (*rps15a* + *nkx2.7* or
379 *rps15a* + *tbx5a*) in comparison to each MO alone (Two-way ANOVA; **Supplemental**

380 **Figure 5D, E**) consistent with the effects observed in *Drosophila*. Together, these results
381 highlight the existence of evolutionarily conserved (fly, zebrafish and hPSC-CMs) genetic
382 interactions between RPs and cardiac TFs genes in the regulation of cardiogenesis.
383 These data also illustrate how the activity of ubiquitously expressed genes such as RPs,
384 can be modulated by cell type-specific genes, like cardiac TFs, to achieve tissue-specific
385 outcomes.

386

387 **RP-regulated HLHS-associated genes control proliferation in a CM-specific manner**

388 Previous studies and this work show that reduced RP function can lead to tissue-
389 specific developmental defects, that in turn can be rescued by loss of p53 [60, 61]. While
390 these findings highlight a downstream role for p53 in the development of RP-dependent
391 phenotypes, they also imply that RPs can regulate cell cycle and/or p53 activity in a
392 tissue-specific manner. Thus, to delineate how RPs might control proliferation in a CM-
393 specific manner, we compared differential gene expression profiles upon the two RP KDs
394 in hPSC-CMs and undifferentiated hPSCs (**Figure 7A**). Consistent with our hypothesis,
395 this analysis revealed that RPs regulate the expression of 493 genes in a CM-specific
396 manner (**Supplemental Tables 5-8**), thereby suggesting the existence of a cell type-
397 specific (cardiac) transcriptional response to RP loss of function.

398 Next, to evaluate whether HLHS-associated genes were part of this lineage-
399 specific transcriptional response, we selected those differentially expressed genes
400 harboring rare and predicted damaging variants in probands from the poor outcome
401 cohort and 75H family (**Supplemental Tables 2, 4)**. Remarkably, this prioritization
402 strategy identified 12 genes potentially associated with HLHS (**Supplemental Table 9**),
403 6 of which were found to also regulate cell cycle activity in hPSC-CMs (**Figure 7B, C**).
404 Thus, collectively this approach led us to identify an RP-dependent and cardiac-specific
405 HLHS-associated gene network that supports CM proliferation *via* the upregulation of
406 *EWSR1, MDC1, PKMYT1* and *KIF1C,* and downregulation of *FAT4* and *EPHA4* (**Figure**
407 **7D, E**).

408 To further explore if RP-regulated HLHS-associated genes control proliferation in
409 a cell type-specific manner, we asked if *EWSR1* KD*,* which elicited the strongest

410 proliferation phenotype in hPSC-CMs, could regulate proliferation in non-cardiac cell
411 types such hPSCs. In contrast to hPSC-CMs, siEWSR1 did not affect the number of
412 OCT4+ cells (**Figure 7F, G**), which suggests that EWSR1 is able to regulate proliferation
413 CM-specifically. EWSR1 is an RNA/DNA binding protein that regulates transcription and
414 RNA splicing and plays a major role as oncogenic driver when fused to ETS transcription
415 factors [62]. In a next step, we tested if EWSR1 regulates CM proliferation by modulating
416 the p53 pathway. Consistent with this hypothesis, immunostaining for p53 downstream
417 target, CDKN1A, revealed that EWSR1 KD both increased the percentage of CDKN1A-
418 positive CMs and decreased EdU incorporation as compared to siControl (**Figure 7H-J**).
419 Consistent with these observations, *RpS15Aa* deficiency fly line placed *in trans* to loss of
420 function allele for *cabeza* (*caz*), the ortholog of *EWSR1,* caused prolongation of systolic
421 interval lengths (**Supplemental Figure 5F)** as compared to controls, suggesting a genetic
422 interaction between these two genes. Collectively, these results support the conclusion
423 that RPs can modulate proliferation in a cell type-specific manner, by controlling the
424 expression of downstream effectors (i.e. *EWSR1*), with a cell type-specific ability to
425 modulate the p53 pathway activity (**Figure 7K and Figure 8**).

426

427 **Discussion**

428 **Implication of ribosomal proteins as genetic modulators in HLHS pathogenesis**
429
430 Recent work, including our own, strongly suggest that defective cardiac
431 differentiation and impaired CM proliferation contribute to HLHS-associated heart defects
432 [16-18]. In this study, we find that ribosomal proteins are critical for maintaining CM
433 proliferation, as well as cardiac structure and function in fish and fly heart models. We
434 show a potential role for RP function in cardiac development and HLHS pathogenesis as :
435 (1) RPs are central regulators of cardiomyocyte proliferation, and (2) RP variants are
436 enriched in a cohort of poor-outcome HLHS patients; (3) a rare predicted-damaging
437 promoter variant in *RPS15A* was associated with HLHS in familial CHD (75H); (4) KD of
438 RPs *in vivo* results in cardiac deficiencies in hPSC-CMs, *Drosophila* and zebrafish, and
439 (5) induces TP53 signaling and blocks proliferation that can be alleviated by inhibition of
440 TP53 in the vertebrate models. Interestingly, the transcriptomic response of a previously

441 reported HLHS proband [18] paralleled these findings and raises the possibility of an
442 underlying ribosomopathy condition in that HLHS family. While universally important for
443 cellular growth, an increasing number of variants in RP genes have been linked to CHD
444 in humans indicating tissue-specific differences in the penetrance of RP gene mutations.
445 Most notably, ~30% of patients with Diamond-Blackfan anemia [63], a ribosomopathy
446 characterized by hypo-proliferative, proapoptotic erythropoiesis, also have CHD. In
447 agreement with another study [46] *rps15a* KD in fish caused a noticeable reduction in
448 circulating red blood cells.

449 In addition to RPS15A, *RpL13* was recently identified as a potential candidate gene
450 involved in CHD from a screen for *de novo* copy number variations (CNVs) in 167 patients
451 with CHD [43]. Furthermore, the Pediatric Cardiac Genomics Consortium (PCGC) exome
452 dataset of 2871 patients with CHD identified several rare, predicted-damaging *de novo*
453 variants in RP genes, 2 of which were found in patients with HLHS [64]. Our finding that
454 RPs genetically interact with core cardiac transcription factors provides a potential
455 mechanism for the cardiac specificity of RP phenotypes. In this context, we hypothesize
456 that RP gene variants might play a role as genetic modifiers (or sensitizers) in the
457 oligogenic pathogenesis of HLHS.
458

459 **Cardiac-specific and RP-dependent regulation of proliferation in the context of**
460 **HLHS**

461 Defective proliferation in left ventricular CMs is a phenotypic hallmark of HLHS [16,
462 17], thereby implying the existence of HLHS-associated mechanisms that regulate
463 proliferation in a CM-specific specific-manner. In this study, we identified RPs as novel
464 candidate genetic regulators of hypoplastic phenotypes observed in HLHS, as 1) rare,
465 predicted damaging variants affecting RP genes are enriched in HLHS probands as
466 compared to healthy controls, 2) KD of most RPs impairs proliferation in hiPSC-CMs
467 (59/80 tested) and heart development in flies (6/6 tested), and 3) systemic loss of *rps15A*
468 function causes heart-specific hypoplastic phenotypes in zebrafish. However, in this
469 context, the evaluation of RPs function in multiple cell types revealed that they are
470 generally required for proliferation (hPSCs, hPSC-CMs and dermal fibroblasts), thus,
471 indicating that RP loss of function triggers a non-cell type specific cell cycle block.

472 Thus, an appealing mechanism by which RP function could be invoked in a
473 spatially restricted manner would involve the regulation of RP expression by cell type-
474 specific TFs. Consistent with this model, all probands harboring RP variants contain
475 mutations affecting their promoter regions (**Table 1**). Also, several of these mutations are
476 predicted to disrupt the binding site of previously identified HLHS-associated TF, ETS1
477 [15, 65]. Consistent with these observations, a recent study from the Bruneau lab [66]
478 show that 38 RP genes are downregulated in TBX5-null hiPSC-CMs and ChIP analysis
479 [67] reveals that a third of these dysregulated RPs (14/38 genes) are bound by TBX5 at
480 their core promoter regions. Thus, we speculate that cell type specific TFs controlling RP
481 expression represent a promising gene class enabling to modulate RP-dependent
482 proliferation in a tissue-specific manner.

483 A second mechanism by which RPs might control proliferation and differentiation
484 in a CM-specific manner, is based on the hypothesis that CMs may be molecularly more
485 sensitive to RP loss-of-function than other cell types. Consistent with this model, RP
486 deficiency predisposes flies, fish and hPSC-CM for interactions with core cardiogenic
487 TFs, including TBX5/*Doc*, GATA4/*pnr* and NKX2-5/*tin*, the latter being the most cardiac
488 restricted. (**Fig.** 6). Moreover, our comparative transcriptomics analysis (**Figure 4**)
489 revealed that RPs regulate gene expression in a CM-specific manner. Among these RP
490 regulated genes, *EWSR1, MDC1, PKMYT1, KIF1C, FAT4 and EPHA4*, were found to be
491 mutated in HLHS families and regulate CM proliferation (**Figure 7**). Remarkably, EWSR1
492 KD did not affect proliferation in hPSCs, while it strongly reduced EdU incorporation in
493 hPSC-CMs, thus suggesting that EWSR1 regulates proliferation in a CM-specific manner.
494 Interestingly, in flies *RpS15Aa* genetically interacts with *cabeza* (*caz,* the fly ortholog of
495 *EWSR1*). Consistent with our observations, a recent study has found that overexpression
496 of a fusion Ewsr1-Fli1 protein in mice specifically induces dilated cardiomyopathy by
497 promoting apoptosis in cardiac myocytes [68]. Similarly, Fat4, a negative regulator of the
498 hippo pathway, which is upregulated upon RP KD, was found to specifically regulate heart
499 size via the regulation of CM size and proliferation [69]. Thus, collectively we propose that
500 RPs represent a central regulatory hub for cell proliferation and differentiation during
501 embryonic development, which can be modulated in a cell type-specific manner by tissue-
502 restricted modulators of RP expression and/or activity.

503

504 **An RP–MDM2–p53/YAP surveillance network in heart development**

505

506 Defects in ribosome biogenesis caused, for example, by reduction in RP gene copy
507 numbers induce a stress response program that activates TP53 (p53) and a cascade of
508 cellular events resulting in apoptosis, inhibition of the cell cycle or DNA damage response
509 (reviewed in e.g. [70]), commonly referred to as nucleolar stress response [71] with
510 activation of TP53 being a key hallmark [72]. A key mechanism involves the release of
511 RPs to the nucleoplasm, where several RPs bind and inhibit MDM2, which again results
512 in p53 stabilization and pathway activation [73, 74]. A recent study showed that RP
513 haploinsufficiency in the developing mouse limb bud also activates a common TP53
514 cascade but results in TP53-dependent tissue-specific changes of the translatome, which
515 might confer the specificity often observed in ribosomopathy [60]. The TP53-MDM2
516 feedback loop is the central molecular node in response to a wide variety of stress signals,
517 including in the human diseased adult heart [75, 76]. As mentioned above, the
518 transcriptomic response of the HLHS family 5H [18] also showed activation of the TP53
519 pathway potentially due to an underlying ribosomopathy. Since low RP levels induce a
520 proliferation blockade that can be overridden by p53-p21/CDKN1A KD, we hypothesize
521 that RP levels may act as signaling components sensing cellular fitness and with a
522 functional outcome either being p53 activation or non-activation. Such an RP–MDM2–
523 p53 surveillance network was previously proposed to be important in response to nutrient
524 availability changes and inhibition of oncogenic activity [77, 78]. Thus, the inhibition of the
525 RP-MDM2-p53 axis might be a therapeutic avenue to consider for functional intervention,
526 although further studies are needed, to identify the upstream mechanisms leading to the
527 *p53* pathway activation observed in HLHS proband cells.

528 Heart-specific KD of the *RpS15Aa* in *Drosophila* causes constriction of larval hearts and
529 atrophy in adult hearts, due to heart loss during metamorphosis, which could not be
530 rescued by p53 reduction, unlike in hPSC-CMs and zebrafish. This might be due to a
531 different, context-dependent role of *p53* in flies previously reported to cause a dwarfing,
532 *Minute*-like phenotype [79]. We hypothesized that the loss of RPs in flies, in conjunction
533 with reduced protein synthesis, might cause nucleolar stress, triggering a cell-intrinsic

534 signaling cascade that prevents the heart to further differentiate and grow. To determine
535 whether cardiac KD of *RpS15Aa* causes nucleolar stress in the *Drosophila* heart, we
536 stained larval hearts for Fibrillarin, a marker for nucleoli and nucleolar integrity. We found
537 that *RpS15Aa* KD causes expansion of nucleolar Fibrillarin staining in cardiomyocyte,
538 which is a hallmark of nucleolar stress (**Suppl. Fig. 6A-C**). As a control, we also
539 performed cardiac KD of *Nopp140*, which is known to cause nucleolar stress upon loss-
540 of-function. We found a similar expansion of Fibrillarin staining in larval cardiomyocyte
541 nuclei (**Suppl. Fig. 6C,D**). This suggests that *RpS15Aa* KD indeed causes nucleolar
542 stress in the *Drosophila* heart, that likely contributes to the dramatic heart loss in adults.

543 The role of the Hippo pathway to regulate cell growth/organ size, proliferation, and
544 survival, and its importance in cardiac biology is conserved between humans and fly [80-
545 83]. The Hippo-YAP pathway is a cell-intrinsic pathway that regulates cardiomyocyte
546 proliferation and thus heart size during development, as demonstrated by the ability of
547 activated Yap to induce postnatal CM regeneration [84]. Interestingly, we find here that
548 overexpression the *Drosophila* ortholog of YAP/TAZ, Yorkie, rescues *RpS15Aa* KD-
549 induced heart loss, dependent on its downstream factor *scalloped* (the *Drosophila*
550 ortholog of *TEAD1/2/3/4)* (Figure **5**). Of note, YAP1 is not only an important regulator of
551 cardiomyocyte proliferation in the embryo but also promotes cardiomyocyte survival and
552 growth in the postnatal heart [85, 86], which is in line with our findings. Interestingly, a
553 proband among the PCGC HLHS patients was transheterozygous for mutations in *RPL15*
554 and *TEAD4* [64], making this an interesting disease candidate pair.

555

556 **Rapid Gene Discovery and Prioritization Approach for Complex Genetic Diseases.**

557 Uncovering the genetic basis of polygenic and heterogeneous diseases, such as HLHS,
558 remains a significant challenge. This difficulty arises from the lack of experimental
559 approaches capable of rapidly determining the role and contribution of genetic variants,
560 as well as their epistatic relationships, in generating disease-associated phenotypes. The
561 current state-of-the-art approach involves using CRISPR-mediated editing or correction
562 of gene variants [87], which is effective for analyzing single-family pedigrees. However,
563 this method is impractical for prioritizing the large number of candidate genes identified

through cohort-wide analyses. Consequently, progress in gene discovery for HLHS has been limited in recent years [12, 88]. In this study, we aimed to address these limitations by employing a HT and unbiased exploration of genes regulating a conserved HLHS-relevant phenotype [41, 89-91], such as reduced CM proliferation, in hiPSCs. Notably, results integration from a whole-genome functional screen in hiPSC-derived CMs (**Figure 1**, RPs are top hits from the screen), genomic data from a HLHS parent-proband cohort (**Figure 2**, RPs represent the most enriched gene class containing rare damaging variants), hiPSC-CM phenotyping from a high value HLHS family (75H), and functional validation in two independent *in vivo* model systems (**Figure 3**), identified RPs as a novel class of HLHS-associated genes. While our study highlights the potential of this approach for gene prioritization, additional research is needed to directly demonstrate the functional consequence of the identified genetic variants, to verify an association between RP encoding genes and HLHS in other patient cohorts with and without poor outcome, and determine if RP variants have a broader role in CHD susceptibility. In conclusion, we propose that the approach outlined in this study provides a novel framework for rapidly prioritizing candidate genes and systematically testing them, individually or in combination, using a CRISPR/Cas9 genome-editing strategy in mouse embryos [33]. Applied in the context of complex genetic diseases, this framework has the potential to yield deeper insights into their underlying mechanisms.

Acknowledgements

This work was supported by a grant from the Wanek Foundation at Mayo Clinic in Rochester, M.N., to J.L.T., T.J.N., T.M.O., R.B. and A.R.C. We gratefully acknowledge the patients and families who participated in this study. We thank Marco Tamayo for excellent technical assistance. This work was supported by National Institutes of Health (R01 HL054732 to R.B.; R01 HL153645, R01 HL148827, R01 HL149992, R01 AG071464

593 to A.R.C.); by California Institute for Regenerative Medicine (DISC2-10110 to A.R.C.); by
594 the American Heart Association (AHA Predoctoral Fellowship 18PRE33960593 to K.B.).

595

596 **MATERIALS AND METHODS**

597 **Key resources table**

Reagent type (species) or resource	Designation	Source or reference	Identifiers	Additional information
Genetic reagent (*D. melanogaster*)	*Hand*$^{4.2}$-Gal4	NA	PMID: 16467358	NA
Genetic reagent (*D. melanogaster*)	R94C02::tdTomato	Y. N. Jan lab	FBtp0137272	NA
Genetic reagent (*D. melanogaster*)	UAS-RpS15Aa^{RNAi}	Vienna Drosophila Resource Center (VDRC)	FBgn0010198	v19198
Genetic reagent (*D. melanogaster*)	Df(RpS15Aa)	Bloomington Drosophila Stock Center (BDSC)	FBab0047266	39614
Genetic reagent (*D. melanogaster*)	UAS-RpL26^{RNAi}	Vienna Drosophila Resource Center (VDRC)	FBgn0036825	v40402 v100280
Genetic reagent (*D. melanogaster*)	UAS-RpL36A^{RNAi}	Vienna Drosophila Resource Center (VDRC)	FBgn0031980	v108391
Genetic reagent (*D. melanogaster*)	UAS-RpS15^{RNAi}	Vienna Drosophila Resource Center (VDRC)	FBgn0034138	v35415 v104439
Genetic reagent (*D. melanogaster*)	UAS-RpL39^{RNAi}	Vienna Drosophila Resource Center (VDRC)	FBgn0023170	v23578 v108821
Genetic reagent (*D. melanogaster*)	UAS-RpL3^{RNAi}	Vienna Drosophila Resource Center (VDRC)	FBgn0020910	v109820
Genetic reagent (*D. melanogaster*)	UAS-yorkie	D. Pan	NA	NA
Genetic reagent (*D. melanogaster*)	UAS-Myc^{RNAi}	Bloomington Drosophila Stock Center (BDSC)	FBgn0262656	25784
Genetic reagent (*D. melanogaster*)	UAS-sd^{RNAi}	Vienna Drosophila Resource Center (VDRC)	FBgn0003345	v101497
Genetic reagent (*D. melanogaster*)	*Df(3L)DocA*	I. Reim	Fbab0037663	NA
Genetic reagent (*D. melanogaster*)	tin^{EC40}	Bloomington Drosophila Stock Center (BDSC)	Fbal0032861	78560

Genetic reagent (*D. melanogaster*)	tin^{346}	Bloomington Drosophila Stock Center (BDSC)	Fbal0035787	92964
Genetic reagent (*D. melanogaster*)	pnr^{VX6}	Bloomington Drosophila Stock Center (BDSC)	Fbal0032468	6334
Genetic reagent (*D. melanogaster*)	Df(pnr)	Bloomington Drosophila Stock Center (BDSC)	Fbab0038315	7982
strain, strain background (*Danio rerio*)	Oregon AB wild-type			A commonly used wildtype strain
strain, strain background (*Danio rerio*)	*Tg(myl7:EGFP)*^{twu277}	Tsai Lab, National Taiwan University	PMID:12950077	A transgenic line of zebrafish labeled with heart-specific EGFP fluorescence.
Strain, strain background (*Danio rerio*)	*Tg(myl7:H2A-mCherry)*^{sd12}	Yelon Lab, University of California, San Diego	PMID:24075907	A transgenic line of zebrafish specifically expressing mCherry in cardiomyocyte nuclei.
Antibody	mouse monoclonal anti-ACTN1	Sigma	A7811	1:800
Antibody	Mouse monoclonal anti-POU5F1 (OCT4)	Sigma	P0082	1:500
Antibody	donkey polyclonal anti-mouse Alexa Fluor 568	Invitrogen	A10037	1:500
Antibody	chicken polyclonal anti-GFP	Aves Labs	GFP-1020	1:300
Antibody	rabbit polyclonal anti-mCherry	Rockland	600-401-P16S	1:200
Antibody	donkey polyclonal anti-chicken AlexaFluor 488	Jackson ImmunoResearch	703-545-155	1:200
Antibody	donkey polyclonal anti-rabbit AlexaFluor 568	Invitrogen	A10042	1:200
other	DAPI (iPSC) 500mg/mL	Sigma	D9542	1:1000
Antibody	mouse anti-Mhc (*Drosophila*)	DSHB	3E8-3D3	1:50
Antibody	anti-mouse-Alexa Fluor 488	Jackson Labs	115-545-003	1:500
other	Alexa Fluor 647 phalloidin	Invitrogen	A22287	1:500
other	DAPI (Zebrafish) 500 mg/mL	Invitrogen	D1306	1:200

Sequence based reagent	RPS15A siRNA	Entrez Gene ID: 6210	Dharmacon	On-Target plus, individual sequence
sequence-based reagent	TP53 siRNA	Entrez Gene ID: 7157	Dharmacon	On-Target plus, Individual Sequence
sequence-based reagent	CDKN1A siRNA	Entrez Gene ID: 1026	Dharmacon	On-Target plus, SmartPool
sequence-based reagent	TP53	371502118c1	IDT Integrated DNA technologies, Coralville, IA	Expression level
sequence-based reagent	CDKN1A	310832423c1	IDT Integrated DNA technologies, Coralville, IA	Expression level
sequence-based reagent	CCNB1	356582356c1	IDT Integrated DNA technologies, Coralville, IA	Expression level
sequence-based reagent	CCNB2	332205979c1	IDT Integrated DNA technologies, Coralville, IA	Expression level
sequence-based reagent	CDK1	281427275c1	IDT Integrated DNA technologies, Coralville, IA	Expression level
sequence-based reagent	MCM2	33356546c1	IDT Integrated DNA technologies, Coralville, IA	Expression level
sequence-based reagent	RPS15A	71772358c2	IDT Integrated DNA technologies, Coralville, IA	Expression level
sequence-based reagent	GAPDH	Hs.PT.45.8326	IDT Integrated DNA technologies, Coralville, IA	Expression level
commercial assay or kit	EdU	Click-it Plus EdU Imaging Kit	Life Technologies	
software, algorithm	Prism v7 and v8		GraphPad Software	

598

599 **Study subjects**

600 Written informed consent was obtained for HLHS probands and family members
601 under a research protocol approved by the Mayo Clinic Institutional Review Board.
602 Cardiac anatomy was assessed by echocardiography. Candidate genes were identified
603 and prioritized by WGS of genomic DNA and RNA sequencing of patient-specific iPSC
604 and cardiomyocytes. Methods for genomic analyses, RNA Sequencing, iPSC technology,

605 bioinformatics and statistics are described in the Online Appendix. Data are available at
606 NCBI GEO database.

607

608

609 **WGS and bioinformatic strategies**

610 Our methods for family phenotyping, WGS, variant filtering, and candidate gene
611 prioritization in the rare HLHS-CHD family and 25 HLHS proband-parent trios have been
612 previously described [7, 9, 18]. In brief, WGS of DNA isolated from blood or cheek swabs
613 was performed on a HiSeq 4000 platform at the Mayo Clinic Medical Genome Facility.
614 BAM files underwent primary and secondary analyses using an established workflow with
615 standard data quality metrics, and reads were aligned to the human hg38 reference
616 genome. Variant call format files with single nucleotide variants and small insertion-
617 deletion (indel) calls were analyzed using Ingenuity Variant Analysis software and
618 knowledge database (Qiagen). To retain only high-confidence data, variants were
619 required to have a base call quality of at least 20 and to pass Variant Quality Score
620 Recalibration. Functionally annotated coding and regulatory variants underwent primary
621 filtering and prioritization by an iterative approach with variants required to have a minor
622 allele frequency (MAF) <0.01 across all races in gnomAD v2.1.[93] Variants predicted to
623 impact protein structure were retained and included missense, frameshift, stop-gain, stop-
624 loss, canonical splice and non-canonical variants predicted to disrupt splicing based upon
625 MaxEntScan[94]. Regulatory variants were defined as those that (a) impact a microRNA
626 or microRNA binding site (b) reside in an enhancer binding site annotated in the VISTA
627 database (http://enhancer.lbl.gov/) or (c) disrupt a predicted promoter or transcription
628 factor binding site informed by the position-weighted matrices available in JASPAR
629 (http://jaspar.cgb.ki.se/). Genes harboring a rare functional variant were further required
630 to have upper quartile cardiac expression during mouse embryonic (e14.5) (Homsy et al.,
631 2015) or human fetal heart development (ranked percentiles from RNASeq experiments
632 available in ENCODE: ENCSR047LLJ (120 day male); ENCSR863BUL (91 day female);
633 ENCSR000AEZ (28 week female and 19 week female) (Davis et al., 2018).
634 For the HLHS-CHD family, a secondary segregation filter was applied to model autosomal
635 dominant inheritance with incomplete penetrance, which required sharing of prioritized

636 rare variants between affected family members. For the poor-outcome HLHS proband-
637 parent trios, a secondary Mendelian filter was applied to identify major-effect driver
638 variants that arose *de novo* or fit recessive modes of inheritance (i.e., homozygosity,
639 hemizygosity, compound heterozygosity).

640 To determine whether certain gene networks were over-represented, two online
641 bioinformatics tools were used. First, STRING[39] was used to investigate experimental
642 and predicted protein-protein and genetic interactions, and clustering of RP genes was
643 demonstrated when the highest stringency filter was applied. In addition, PANTHER[38]
644 was employed to identify potential enrichment of genes by ontology classification.

645

646 **Generation of hPSC-VCMs**

647 Id1 overexpressing hPSCs [33, derived from, 95] were dissociated with 0.5 mM
648 EDTA (ThermoFisher Scientific) in PBS without $CaCl_2$ and $MgCl_2$ (Corning) for 7 min at
649 room temperature. hPSC were resuspended in mTeSR-1 media (StemCell Technologies)
650 supplemented with 2 μM Thiazovivin (StemCell Technologies) and plated in a Matrigel-
651 coated 12-well plate at a density of 3 x 10^5 cells per well. After 24 hours after passage,
652 cells were fed daily with mTeSR-1 media (without Thiazovivin) for 3-5 days until they
653 reached ≥ 90% confluence to begin differentiation. hPSC-VCMs were differentiated as
654 previously described [95]. At day 0, cells were treated with 6 μM CHIR99021 (Selleck
655 Chemicals) in S12 media [96]. for 48 hours. At day 2, cells were treated with 2 μM Wnt-
656 C59 (Selleck Chemicals), an inhibitor of WNT pathway, in S12 media. 48 hours later (at
657 day 4), S12 media is fully changed. At day 5, cells were dissociated with TrypLE Express
658 (Gibco) for 2 min and blocked with RPMI (Gibco) supplemented with 10% FBS (Omega
659 Scientific). Cells were resuspended in S12 media supplemented with 4 mg/L
660 Recombinant Human Insulin (Gibco) (S12+ media) and 2 μM Thiazovivin and plated onto
661 a Matrigel-coated 12-well plate at a density of 9 x 10^5 cells per well. S12+ media was
662 changed at day 8 and replaced at day 10 with RPMI (Gibco) media supplemented with
663 213 μg/μL L-ascorbic acid (Sigma), 500 mg/L BSA-FV (Gibco), 0.5 mM L-carnitine
664 (Sigma) and 8 g/L AlbuMAX Lipid-Rich BSA (Gibco; CM media). Typically, hPSC-ACMs
665 start to beat around day 10. At day 15, cells were purified with lactate media (RPMI

666 without glucose, 213 µg/µL L-ascorbic acid, 500 mg/L BSA-FV and 8 mM Sodium-DL-
667 Lactate (Sigma), for 4 days. At day 19, media was replaced with CM media.

668 **siRNA transfection, proliferation assay and immunostaining in hPSC-VCMs**

669 At day 25 of differentiation, hPSC-VCMs were dissociated with TrypLE Select 10X
670 (Gibco), 10 min and neutralized with RPMI supplemented with 10% FBS. Cells were
671 resuspended in RPMI with 2% KOSR (Gibco) and 2% B27 50X with vitamin A (Life
672 Technologies) supplemented with 2 µM Thiazovivin and plated at a density of 5,000
673 cells/well in a Matrigel-coated 384-well plate. hPSC-VCMs were transfected with siRNA
674 (Dharmacon: ON-TARGETplus, custom RNAi cherry-pick libraries 0.1 nmol). For the
675 whole genome screening, siRNAs directed to 18,000 human genes were purchased from
676 the Genomic Center Facility at SBP at a final concentration of 25 nM using lipofectamine
677 RNAiMax (ThermoFisher) and opti-MEM (Gibco). 48 hours post-transfection, cells were
678 labelled with 10 µM EdU (ThermoFisher). After 24h of EdU incubation, cells were fixed
679 with 4% paraformaldehyde for 30 min and blocked in blocking buffer (10% Horse Serum,
680 10% Gelatin and 0.5% Triton X-100) for 20 min. EdU was detected according to protocol
681 and cells were stained with cardiac specific marker ACTN2 (A7811, Sigma, dilution
682 1/800), secondary antibody Alexa Fluor 568 (Invitrogen, 1/500) and DAPI (1/1000) in
683 Blocking Buffer. Cells were imaged with ImageXpress Micro XLS microscope (Molecular
684 Devices) and custom algorithms were used to quantify % of EdU+ ACTN1+ hPSC-VCMs
685 and the number of ACTN1+ cells. To quantify TP53 levels in hPSC-VCMs, cells were
686 stained with Phospho-p53 (700439, ThermoFisher, 1/500), counterstained with ACTN1
687 (anti-mouse A7811, Sigma, or anti-rat ab50599, Abcam), and imaged and quantified with
688 ImageXpress microscope. Whole genome screening was performed in one-replicate. All
689 the other siRNAs experiments were performed in quadruplicates.

690 **RNA-seq and data analysis**

691 hPSCs and hPSC-derived CMs were transfected with 25nM final concentrations of siRNA
692 against RPS15A, RPL39 and with scrambled control siRNAs as above. 2 days after
693 siRNA transfection RPs KD were verified and confirmed by proliferation assay (see
694 above), and cells were pelleted and resuspended in 500µl TRIzol reagent followed by

695 total RNA extraction. Library preparation and sequencing of the samples was done at La
696 Jolla Institute of Immunology (La Jolla, CA). FASTQ files were processed using nf-
697 core/rnaseq (version 21.03.0.edge [97]). Differential gene expression was determined
698 using R/DESeq2 [98] and GO term enrichment was done using gprofiler2[99]. Analysis
699 scripts can be downloaded at github.com/gvogler. Raw reads and counts tables are
700 available at GEO accession number GSE207658.

701

702 **Proliferation assay in parent/proband iPSCs**

703 hPSCs were dissociated as described previously and plated in a Matrigel-coated
704 384-well plate at a density of 3,000 cells per well. Cells were transfected with siRNA at a
705 final concentration of 25nM using lipofectamine RNAiMax and opti-MEM. After 3 days,
706 cells were labelled with 10 μM EdU for 1 hour. Cells were fixed with 4% paraformaldehyde
707 for 30 min and blocked in blocking buffer for 20 min. EdU was detected according to the
708 protocol and stained with stem cell specific marker OCT4 (P0082, Sigma, 1/500),
709 secondary antibody Alexa Fluor 568 and DAPI in Blocking Buffer. Cells were imaged with
710 ImageXpress microscope and % of EdU+ cells and number of OCT4+ cells were
711 quantified.

712 **Quantitative Real Time PCR (RT-qPCR) in parent/proband iPSCs and hPSC-CMs**

713 Total RNA was extracted using TRIzol and chloroform. 1ug of RNA was converted
714 in cDNA using QuantiTect Reverse Transcription kit (Qiagen). qRT-PCR was performed
715 using SYBR green (Biorad). Human primers sequences for qRT-PCR were obtained from
716 Harvard Primer Bank: TP53 (Primer Bank ID: 371502118c1), CDKN1A (Primer Bank ID:
717 310832423c1), CCNB1 (Primer Bank ID: 356582356c1), CCNB2 (Primer Bank ID:
718 332205979c1), CDK1 (Primer Bank ID: 281427275c1), MCM2 (Primer Bank ID:
719 33356546c1), RPS15A (Primer Bank ID: 71772358c2). All values were normalized to
720 *GAPDH (Primer Bank ID: 378404907c1)*. At least 3 independent biological replicates
721 were performed for each experiment.

722 **Statistical analysis**

723 To determine any statistical significance between experimental and control groups
724 in hPSC-VCMs and iPSCs from parent/proband trio, we calculated two-sided p values
725 with Student's t-test using GraphPad Prism 8.1.2 software.

726

727 ***Drosophila* heart function studies**

728 *Drosophila* orthologs were determined using the DIOPT database [100], and fly
729 stocks were obtained from the Vienna Drosophila Resource Center (VDRC) stock center
730 or Bloomington Drosophila Stock Center (BDSC) as indicated in the key source table. For
731 *in vivo* functional heart analysis, we developed a high-throughput method based on
732 genetically modified flies with cardiomyocyte-specific RFP fluorescence (Klassen et al.).
733 The reporter line by itself or combined with the heart-specific *Hand*$^{4.2}$-Gal4 driver
734 (including all cardioblasts/cardiomyocytes, pericardial cells and wing hearts throughout
735 development starting at post-mitotic, mid-embryonic stages through adulthood [101-103]
736 was crossed to UAS-lines or mutant flies. For interaction studies a fly line harboring the
737 fluorescent reporter, *Hand*$^{4.2}$-Gal4 driver and a Deficiency for RpS15Aa was generated.
738 Adult progeny flies were immobilized and exposed to fluorescence light to record 5 sec
739 high frame rate movies of the beating heart. Movies were analyzed by fully automated
740 quantification of contractility and rhythmicity parameters of the heart [104]. Semi-intact
741 adult fly hearts were filmed and analyzed according to standard protocol [27, 105].

742

743 **Immunostainings of the fly heart**

744 The immunostaining of fly adult hearts was performed as described previously
745 [106]. In short, adult flies were dissected in a semi-intact fashion to expose the heart
746 according to protocol [27, 107]. Myofibrils were relaxed using 10mM EGTA followed by
747 fixation in 4% formaldehyde for 15 min. Hearts were washed with PBS + Triton (PBT;
748 0.03 % triton X-100) and stained using Alexa 647 phalloidin (Life Technologies) 2h at
749 room temperature (RT). For Mhc labelling, hearts were stained using anti-Mhc antibody
750 (1:50, incubation over night at 4°C) and after three washes with PBT, secondary antibody
751 was applied for 2 h at RT. Hearts were washed with PBT three times and PBS one time
752 and mounted using ProLong Gold mountant with DAPI (Life Technologies). Heart

753 preparations were imaged with the Imager.Z1 with an Apotome (Carl Zeiss), Hamamatsu
754 Orca Flash 4.0 and ZEN imaging software (Carl Zeiss).
755
756
757 **Zebrafish Husbandry**
758 All zebrafish experiments were performed in accordance with protocols approved
759 by IACUC. Zebrafish were maintained under standard laboratory conditions at 28.5°C. In
760 addition to Oregon AB wild-type, the following transgenic lines were used:
761 *Tg(myl7:EGFP)*^{twu277} [108] and *Tg(myl7:H2A-mCherry)*^{sd12} [109].
762 In zebrafish, gene expression was manipulated using standard microinjection of
763 morpholino (MO) antisense oligonucleotides [110]. In addition, we performed targeted
764 mutagenesis using CRISPR/Cas9 genome editing[111-113], to create insertion/deletion
765 (INDEL) mutations in relevant ribosomal genes (F0). Subsequently, zebrafish were raised
766 to 72 hours post fertilization (hpf), immobilized in low melt agarose and the hearts were
767 filmed and analyzed according to standard protocol[27].
768
769 **MO sequence information:**
770 All MOs were purchased from Gene Tools, LLC, synthesized at 300nmol, except
771 zebrafish p53 oligos at 100nmol.
772 Zebrafish *rpl13* 5'-UTR MO: TTGTTCACTCCGTCCTTAGCGGAAA
773 Zebrafish *rps15a* 5'-UTR MO: CGCACCATGATGCCAGTTCTGCAAT
774 Zebrafish *rpl39* 5'-UTR MO: GGATCGCAATCCGTTCACCACTATG
775 Zebrafish p53 MO: GCGCCATTGCTTTGCAAGAATTG
776 Zebrafish Control MO: 5'-CCT CTT ACC TCA GTT ACA ATT TAT A-3'.
777
778 **Zebrafish SOHA (Semi-automated Optical Heartbeat Analysis)**
779 Larval zebrafish (72 hpf) were immobilized in a small amount of low melt agarose
780 (1.5%) and submerged in conditioned water. Beating hearts were imaged with direct
781 immersion optics and a digital high-speed camera (up to 200 frame/sec, Hamamatsu

782 Orca Flash) to record 30 seconds movies; images were captured using HC Image
783 (Hamamatsu Corp.). Cardiac function was analyzed from these high-speed movies using
784 semi-automatic optical heartbeat analysis software[27, 114], which for zebrafish
785 quantifies heart period (R-R interval), cardiac rhythmicity, as well as chamber size and
786 fractional area change. All hearts were imaged at room temperature (20-21°C). Statistical
787 analyses were performed using Prism software (Graphpad). Significance was determined
788 using two-tailed, unpaired student t-test or one-way ANOVA and Dunnett's multiple
789 comparisons post hoc test as appropriate.

790 **Zebrafish Cardiomyocyte Cell Counts and Cardiac immunofluorescent imaging**

791 To count cardiomyocytes, we used the expression of H2AmCherry in the nuclei
792 (*Tg(myl7:H2A-mCherry)*[109] to qualify as an individual cell, performed the "Spot" function
793 in Imaris to distinguish individual cells in reconstructions of confocal z-stacks.[115, 116]
794 To compare data sets, we used Prism software (GraphPad) to perform Student's t-test
795 with two-tail distribution. Graphs display mean and standard deviation for each data set.

796 Whole-mount immunofluorescence was performed as previously described[18,
797 115-117] (see also key resources table). Confocal imaging was performed on an LSM
798 710 confocal microscope (Zeiss, Germany) with a 40x water objective. Exported z-stacks
799 were processed with Imaris software (Bitplane), Zeiss Zen, and Adobe Creative Suite
800 software (Photoshop and Illustrator 2020). All confocal images shown are projection
801 views of partial reconstructions from multiple z-stack slices, except where noted that
802 images are views of a single slice.

803 For proliferation assays, embryos at 24, 48, and 72 hpf were fixed in 4%
804 paraformaldehyde overnight at 4 °C, washed in PBS with 0.1% Tween-20 (PBST).
805 Samples were blocked in 5% normal goat serum in PBST prior to incubation with primary
806 antibodies. Proliferating cells were labeled with anti-phospho-histone H3 (Sigma Aldrich-
807 H0412 PH3; 1:500) and total nuclei were counterstained with DAPI. Embryos were
808 mounted in ProLong Gold for imaging. Whole-mount hearts were imaged on a Zeiss
809 Apotome microscope at 10× magnification. Z-stacks were acquired and reconstructed
810 using Fiji/ImageJ. Regions corresponding to atrium, ventricle, atrioventricular canal, and
811 outflow tract were manually segmented. For some experiments, cardiomyocyte nuclei

812 were identified based on Tg(myl7:H2A-mCherry) expression, with DAPI used to quantify
813 total cell counts. For proliferation experiments DAPI was used to identify cardiac cells and
814 proliferating cells were identified by PH3 staining. Proliferative indices were calculated as
815 PH3+/DAPI+ ratios from z-stacks analyzed in Fiji/ImageJ using the Cell Counter plugin.
816 Cell counts were performed on at least 10 embryos per condition per timepoint.

817

818

819 **Zebrafish CRISPR/Cas9 experiments**

820 Detailed steps were previously described[118] and we followed IDT manufacture
821 instruction for Complexes preparation. crRNA:tracrRNA Duplex Preparation: Target-
822 specific Alt-R® crRNA (sequence information see below) and common Alt-R® tracrRNA
823 were synthesized by IDT and each RNA was dissolved in duplex buffer (IDT) as 100 μM
824 stock solution. Stock solutions were stored at -20°C. To prepare the crRNA:tracrRNA
825 duplex, equal volumes of 100 μM Alt-R® crRNA and 100μM Alt-R® tracrRNA stock
826 solutions were mixed together and annealed by heating followed by gradual cooling to
827 room temperature by manufacture instruction: 95°C, 5 min on PCR machine; cool to
828 25°C; cool to 4°C rapidly on ice. The 50 μM crRNA:tracrRNA duplex stock solution was
829 stored at -20°C. Preparation of crRNA:tracrRNA:Cas9 RNP Complexes: Cas9 protein
830 (Alt-R® S.p. Cas9 nuclease, v.3, IDT) was adjusted to 25 μM stock solution in 20mM
831 HEPES-NaOH (pH 7.5), 350 mM KCl, 20% glycerol, dispensed as 8 ul aliquots, and
832 stored at -80°C. 25μM crRNA:tracrRNA duplex was produced by mixing equal volumes
833 of 50 μM crRNA:tracrRNA duplex stock and duplex buffer (IDT). We used 5 μM RNP
834 complex. To generate 5μM crRNA:tracrRNA:Cas9 RNP complexes: 1 μl 25 μM
835 crRNA:tracrRNA duplex was mixed with 1 μl 25 μM Cas9 stock, 2 μl H2O, and 1 μl 0.25%
836 phenol red solution. Prior to microinjection, the RNP complex solution was incubated at
837 37°C, 5 min and then placed at room temperature. Approximately one nanoliter of 5 μM
838 RNP complex was injected into the cytoplasm of one-cell stage embryos to generate F0
839 larva.

840

841 **IDT crRNA sequence information:**

842 All crRNAs were purchased from Integrated DNA Technologies, Inc., synthesized
843 at 2 nmol with standard desalting condition.

844 Dr.Cas9.RPS15A.1.AC: /AltR1/rUrU rGrUrU rGrUrC rArArU rCrUrC rArCrA rGrGrG
845 rGrUrU rUrUrA rGrArG rCrUrA rUrGrC rU/AltR2/

846 Dr.Cas9.RPS15A.1.AB: /AltR1/rGrC rGrUrA rCrUrA rUrGrA rCrUrU rUrArG rArGrC
847 rGrUrU rUrUrA rGrArG rCrUrA rUrGrC rU/AltR2/

848 Dr.Cas9.RPS17.1.AC:
849 /AlTR1/rUrGrArCrUrUrCrCrArCrArUrUrArArCrArArGrCrGrUrUrUrUrArGrArGrCrUrArUrG
850 rCrU/AlTR2/

851 Dr.Cas9.RPS28.1.AA:
852 /AlTR1/rCrUrGrGrGrArArGrArArCrUrGrGrCrUrCrCrCrArGrUrUrUrUrArGrArGrCrUrArUr
853 GrCrU/AlTR2/

854

855

856

857 **Competing interests:** None.

858

859

860 **Table 1: Table 1 – Variants in ribosomal genes in HLHS probands.** Abbrevations:
861 MAF – minor allele frequency; TFBS – transcription factor binding site; n.t. – not tested;
862 ASD – atrial septal defect; PLE - Protein-losing enteropathy; RV – right ventricle; RVEF
863 – right ventricular ejection fraction; RVEDP - right ventricular end diastolic pressure

864

865 **Figure 1: Whole Genome siRNA Screen identified Ribosomal proteins as agonists**
866 **of cardiomyocyte proliferation. (A)** High-throughput iPSC-derived CM proliferation
867 screen overview. **(B)** Screen result showing normalized % EdU+ CMs (X-axis) and
868 relative total number of CMs (Y-axis) upon knockdown of genome-wide siRNAs (18,055
869 siRNAs). siRNAs for RPL and RPS genes highlighted in red. **(C)** Representative
870 immunofluorescence images of proliferation (EdU incorporation, green, CM marker
871 ACTN2, red) of induced hPSC-CMs upon *TP53* and *RPS14* knockdown. Insets: nuclei
872 (DAPI) **(D)** Gene ontology enrichment analysis for WGS hits (BP, biological process;
873 FDR-corrected analysis using gprofiler2). (**E**) Overview of hits corresponding to top 4 non-
874 redundant BP categories.

875

876 **Figure 2: Ribosomal gene variants identified in HLHS. (A)** Gene prioritization scheme
877 of 25 poor-outcome proband-parent trios. **(B)** Testing 292 HLHS candidate genes from
878 all poor-outcome families in CMs identified RPs as major regulators of hPSC-CM
879 proliferation (Normalized fraction of ACTN2+/EdU+ cells). **(C)** *Drosophila* cardiac
880 phenotypes induced by loss of RP genes affected in HLHS patients with poor outcome.
881 Heart is visualized by RFP expression specifically in cardiomyocytes (R94C02::tdTom).
882 Knockdown is achieved by sustained Gal4/UAS activity using Hand4.2-Gal4. (**D**) Wild-
883 type zebrafish larva, *rps17* and *rps28* CRISPR mutants and *rpl39* morphants at 72 hpf.
884 *rpl39* morphants, injected with 1 ng MO in lateral view, show mild edema. **(E)** Systolic
885 surface area (SA) upon *rps17* and *rps28* CRISPR, and diastolic SA after *rpl39* MO in the
886 atrium and ventricle of zebrafish hearts.

887 **Figure 3: Characterization of RPS15A from 75H HLHS index family. (A) (B) (C)**
888 Prioritized candidate genes from the 75H family and relative hPSC-CM proliferation
889 capacity upon KD. (**D**) Representative immunofluorescence images of proliferation (EdU

890 incorporation, green; CM marker ACTN2, red) of induced hPSC-CMs upon siRPS15A
891 knockdown. **(E)** Heart-specific KD of *RpS15Aa* in *Drosophila* adult hearts cause loss of
892 heart tissue and is fully penetrant. **(F)** Representative immunofluorescence images of
893 control and *RpS15Aa*-RNAi shows partial heart loss (Myosin heavy chain, Mhc, red; heart
894 tissue-reporter, green). **(G)** CRISPR-mediated loss of *rps15a* in F_0 larval zebrafish hearts
895 causes decrease in CM number. **(H)** Representative immunofluorescence of hearts and
896 whole-mount images of control and *rps15a*-CRISPR F_0 larval hearts (CM nuclei reporter,
897 red).

898
899
900 **Figure 4***:* **Loss of ribosomal gene function in CMs invokes TP53-stress response**.
901 **(A)** RNA sequencing of hPSC-CMs following siRNA-treatment for *RPL39* and *RPS15A*
902 shows both, convergent and divergent transcriptomic response. **(B)** GO term analysis of
903 differentially expressed genes following RP KD shows TP53-mediated response,
904 including upregulation of *CDKN1A*. **(C, D)** CDKN1A is highly upregulated in CMs following
905 *siRPS15A* treatment. **(E, F)** Reduced CM proliferation upon *RPS15A* KD is mediated by
906 *CDKN1A*/*TP53* and can be rescued upon their co-KD. **(G, H)** Larval zebrafish CM number
907 is reduced by morpholino-treatment for rps15a and can be attenuated by P53 morpholino
908 co-injection. Control and morphant (MO) hearts of 72 hpf zebrafish larva stained with
909 *Tg(myl7:EGFP)* and *Tg(myl7:H2A-mCherry)*. Note that smaller heart with aberrant
910 looping by *rps15a* MO is partially reversed by *p53* co-KD. Student's t-test, *p<0.05,
911 **p<0.01, ***p<0.001, ****p<0.0001**.**
912
913 **Figure 5: Rescue of *RpS15Aa* KD-mediated heart tube loss in Drosophila by**
914 **YAP/yorkie overexpression depending on its co-factor TEAD/scalloped. (A)**
915 Representative images of RFP expressing fly hearts. RpS15Aa KD-mediated heart tube
916 loss can be partially rescued by overexpression of *yorkie* (*RpS15Aa* RNAi + *yorkie* OE) .
917 The rescue by *yki* OE depends on its co-factor *sd*. Flies were raised at 25 °C. **(B)**
918 Quantification of events presented as a percentage of flies exhibiting whole heart tube
919 versus partial heart loss (defined as 25-75% heart tube length compared to wildtype) or
920 no heart tube. Statistics: Fisher's exact test, *p<0.05. **(C)** Proposed signaling cascade

921 underlying cardiac growth, proliferation and differentiation impairment following ribosomal
922 stress (adapted from Baker et al., 2019).

923

924 **Figure 6: *RPS15A* genetically interacts with cardiac transcription factors. (A)** The
925 majority of cardiac transcription factors do not impact CM proliferation, except for e.g.,
926 HES4 and HOPX. **(B)** *TBX5* genetically interacts with *RPS15A* and *RPL39*. *siTBX5* does
927 not impact CM proliferation at 0.5, 1, 1.5 or 2nM si-concentration, and neither do
928 *siRPS15A* and *siRPL39* alone at 0.5nM. CM proliferation is reduced in siRP backgrounds
929 with increased titration of *siTBX5*. Two-way ANOVA for si*TBX5* dosage, RP-knockdown
930 and their interaction. **(C)** Representative fly heart segment (A4) from control flies,
931 heterozygous mutants ($tin^{346/+}$, $pnr^{VX6/+}$, $Doc^{Df/-}$, $Df(RpS15Aa)^{+/-}$) and transheterozygous
932 mutants. $tin^{+/-} = tin^{346}/+$, $pnr^{+/-} = Df(pnr)/+$, $Doc^{+/-} = Df(DocA)/+$. Note the deformation and
933 myofibrillar disorganization in the transheterozygous mutants. **(D)** Quantification of adult
934 *Drosophila* heart defects and genetic interaction. - Statistics: Fisher's exact test on
935 absolute numbers testing *normal* vs. *severely deformed* hearts. *p<0.05, **p<0.005,
936 ***p<0.001.

937

938 **Figure 7: RP-dependent cardiac-specific regulation of cell proliferation. (A)**
939 Schematic illustrating approach to identify novel RP-dependent and cardiac-specific
940 HLHS-associated gene network controlling CM proliferation. **(B)** Heatmap showing
941 differential expression (hiPSC-CMs vs hiPSCs) of genes regulating CM proliferation. **(C)**
942 Histogram showing effect of cardiac-specific and HLHS-associated genes on CM
943 proliferation. **(D)** Visualization of RP-dependent and cardiac-specific HLHS-associated
944 gene network (GeneMania). HLHS families. **(E)** Table of HLHS families harboring rare
945 and damaging variant in RP-dependent and cardiac-specific genes. **(F)** Histogram
946 showing lack of effect of siEWSR1 on OCT4+ hiPSCs. **(G)** Representative images of
947 OCT4+ cells in siControl and siEWSR1. **(H)** Histogram showing that siEWSR1 increases
948 the % of CDKN1A+ CMs as compared to siControl. **(I)** Histogram showing that siEWSR1
949 concomitantly decreases the % of EDU+ CMs as compared to siControl. **(J)**
950 Representative images showing immunostaining for CDKN1A (white), EDU (green) and

951 ACTN2 (Red) in siEWSR1 an siControl condition. **(K)** Pathway reconstruction of cardiac
952 and RP-dependent regulation of CM proliferation by HLHS-associated genes. Chi-square
953 test, *p<0.05, **p<0.005, ***p<0.001

954

955 **Figure 8: Model for RP-dependent involvement in HLHS-associated phenotypes**.
956 Schematic showing that combined prioritization and unbiased screening led to the
957 identification of a novel HLHS-associated gene network regulating CM proliferation as
958 potential disease-causing mechanism.

959

960 **Supplemental Figure 1: (A, B)** Confirmatory siRNA screening for all RP genes confirms
961 critical role for RPs in CM proliferation. (**C, D**) KD of RPs reduces proliferation in human
962 fibroblasts.

963

964 **Supplemental Figure 2: Model organism phenotypes caused by loss of RP genes.**
965 **(A)** Pedigree of the extended 75H family investigated for shared variants between HLHS
966 proband (black square) and distant cousin with CHD (half-filled circle). (**B**) **(C)** Diastolic
967 and **(D)** and Systolic Surface Area after rps15a CRISPR. Statistics: Mann-Whitney test,
968 *p<0.05, **p<0.01, ***p<0.001, ****p<0.0001

969

970 **Supplemental Figure 3: *rps15a* zebrafish larval morphants show heart dysfunction**
971 **and reduction in cardiomyocyte number. (A)** Lateral view (head to the right) of a wild-
972 type control zebrafish larva (top) and a morphant (bottom) following injection of 2 ng/µl
973 *rps15a* morpholino (MO). The morphant exhibits near normal body/tail but notable
974 pericardial edema (arrowhead). **(B)** Control (left) and morphant hearts (right) stained with
975 Tg(*myl7*:*EGFP*) and Tg(*myl7*:*H2A-mCherry*). Note the smaller heart with aberrant looping
976 in morphant heart. **(C)** Total CM counts (mCherry+ cells) in control and *rps15a* morphants
977 shown in (B). **(D)** Fractional area change (FAC) in control and *rps15a* morphants. **(E-H)**
978 Injection of Control MO had little effect on zebrafish cardiac function. There was no
979 significant difference between uninjected and injected controls with respect to (**E**) Systolic

980 or (**F**) Diastolic Surface Areas, (**G**) Fractional Area Change or (**H**) R-R intervals. Student's
981 t-test, *p<0.05, **p<0.01, ***p<0.001, ****p<0.0001.
982
983 **Supplemental Figure 4: Proliferation and heart function depends on RPS15A and**
984 **is regulated via TP53 in CMs and zebrafish. (A-C)** Cardiac proliferation (by PH3, **A**),
985 total CM number (DAPI, **B**) and ratio of proliferating CMs (C) assessed for *rps15a*
986 morphants (KD) and CRIPSR (KO) for three timepoints, 24/48/72hpf **(D, E)** The number
987 of *siRPS15A*-treated CMs is strongly reduced, which can be attenuated by co-KD of
988 *CDKN1A* or *TP53*. **(F,G)** Loss of *rps15a* causes strong reduction in zebrafish heart
989 contractility (measured by Fractional Area Change, **C**) and heart period **(D)**, which can be
990 rescued by co-KD of *p53* in both, zebrafish heart atrium and ventricle.
991
992 **Supplemental Figure 5: Genetic interaction between *RpS15Aa/RPS15A* and**
993 ***cabeza/EWSR1* (A, B)** Dose-dependent inhibition of hPSC-CMs proliferation by RPS15A
994 KD. **(C)** Diastolic Diameter (DD), and Heart Period (HP) of 3-week-old female control and
995 heterozygous RpS15Aa deficient flies with or without additional heterozygous mutation in
996 tinman, pannier or Dorsocross. Statistics: Kruskal-Wallis, *p<0.05, **p<0.005, ***p<0.001,
997 ****p<0.0001. Note, the prolonged HP in transheterozygous mutants for Df(RpS15Aa)
998 and tinman. **(D, E)** FAC, and HP of the atria and ventricles at 72 hpf in zebrafish embryos
999 injected with 0.5 ng rps15a and/or 1 ng nkx2.7 MOs (**E**) or 0.5 ng rps15a and/or 0.5 ng
1000 tbx5 MOs (F**).** Note, that FAC and heart periods show synergistic genetic interaction
1001 between rps15a and nkx2.7 and tbx5a. Statistics: 2-Way ANOVA, *p<0.05, **p<0.01,
1002 ****p<0.0001.**(F)** Systolic intervals (SI) of 1-week-old adult flies upon heart-specific
1003 knockdown of *cabeza* (*caz*^{32990} or *caz*^{34839} RNAi) using Hand$^{4.2}$-Gal4 driver with or without
1004 additional RpS15Aa heterozygosity (RpS15Aa$^{Df/+}$) and age-matched controls. Automated
1005 analysis of SI depicted as median with interquartile range obtained from 5s high-frame-
1006 rate videos. Statistics: Kruskal-Wallis test, *p<0.05, **p<0.01, ***p<0.001.
1007
1008 **Suppl. Fig. 6: RpS15Aa KD induces nucleolar stress in 3rd instar larval hearts. (A)**
1009 Nucleolar stress induction in 3rd instar larval hearts upon *RpS15Aa* KD as indicated by
1010 enlarged nucleoli. Hearts from control and *RpS15Aa* KD. 3rd instar larva stained for F-

1011 Actin (red), DAPI (blue), and nucleolus marker Fibrillarin (green) and cardiomyocyte (CM)
1012 nuclei in magnifications. Note, heart constriction upon *RpS15Aa* KD in the larval heart.
1013 **(B)** Quantification of nucleolus area and area ratio(nucleolus/nucleus) indicates
1014 significantly enlarged nucleoli upon *RpS15Aa* KD. Statistics: Mann-Whitney test,
1015 ****p<0001. **(C)** Schematic representation of different nucleolar phenotypes upon RNAi-
1016 mediated loss of function. **(D)** As a positive control, KD of another nucleolar key player
1017 *Nopp140* specifically in the heart using Hand$^{4.2}$-Gal4 combined with Fibrillarin^{EGFP} (kind
1018 gift of the Wieschaus lab) leads to loss of nucleolar maintenance. 3rd instar larva stained
1019 for F-Actin (red) and DAPI (blue). Fibrillarin in (green). Cardiomyocyte nuclei in
1020 magnifications. PC= Pericardial Cell
1021
1022

1023 **Supplemental Table 1: Whole genome siRNA screen results table.**

1024 **Supplemental Table 2: 292 filtered variants from poor-outcome HLHS probands.**
1025 MOI – mode of inheritance

1026 **Supplemental Table 3: Subset from all 292 genes that cause CM proliferation**
1027 **defects and/or fly heart defects**

1028 **Supplemental Table 4: Segregating variants of 75H proband.**

1029 **Supplemental Tables 5-8: Differential gene expression lists for siRPL39 and**
1030 **siRPS15A in hPSCs and CMs.**

1031 **Supplemental Table 9: 12 genes prioritized after RNAseq and WGS analysis.**

1032

1033

1034

1035

1036

1038 **REFERENCES**

1039 1. Gordon BM, Rodriguez S, Lee M, Chang R-K. Decreasing number of deaths of infants
1040 with hypoplastic left heart syndrome. J Pediatr. 2008;153(3):354-8. doi:
1041 10.1016/j.jpeds.2008.03.009.
1042 2. Reller MD, Strickland MJ, Riehle-Colarusso T, Mahle WT, Correa A. Prevalence of
1043 congenital heart defects in metropolitan Atlanta, 1998-2005. J Pediatr. 2008;153(6):807-13. doi:
1044 10.1016/j.jpeds.2008.05.059.
1045 3. Crucean A, Alqahtani A, Barron DJ, Brawn WJ, Richardson RV, O'Sullivan J, et al. Re-
1046 evaluation of hypoplastic left heart syndrome from a developmental and morphological
1047 perspective. Orphanet J Rare Dis. 2017;12(1):138. doi: 10.1186/s13023-017-0683-4.
1048 4. Konno Y, Toki T, Tandai S, Xu G, Wang R, Terui K, et al. Mutations in the ribosomal
1049 protein genes in Japanese patients with Diamond-Blackfan anemia. Haematologica.
1050 2010;95(8):1293-9. doi: 10.3324/haematol.2009.020826.
1051 5. Agopian AJ, Goldmuntz E, Hakonarson H, Sewda A, Taylor D, Mitchell LE, et al.
1052 Genome-Wide Association Studies and Meta-Analyses for Congenital Heart Defects. Circ
1053 Cardiovasc Genet. 2017;10(3):e001449. doi: 10.1161/CIRCGENETICS.116.001449.
1054 6. Martin LJ, Pilipenko V, Benson DW. Role of Segregation for Variant Discovery in
1055 Multiplex Families Ascertained by Probands With Left Sided Cardiovascular Malformations.
1056 Front Genet. 2018;9:729. doi: 10.3389/fgene.2018.00729.
1057 7. Theis JL, Hrstka SCL, Evans JM, O'Byrne MM, de Andrade M, O'Leary PW, et al.
1058 Compound heterozygous NOTCH1 mutations underlie impaired cardiogenesis in a patient with
1059 hypoplastic left heart syndrome. Hum Genet. 2015;134(9):1003-11. doi: 10.1007/s00439-015-
1060 1582-1.
1061 8. Elliott DA, Kirk EP, Yeoh T, Chandar S, McKenzie F, Taylor P, et al. Cardiac homeobox
1062 gene NKX2-5 mutations and congenital heart disease: associations with atrial septal defect and
1063 hypoplastic left heart syndrome. J Am Coll Cardiol. 2003;41(11):2072-6. doi: 10.1016/s0735-
1064 1097(03)00420-0.
1065 9. Theis JL, Zimmermann MT, Evans JM, Eckloff BW, Wieben ED, Qureshi MY, et al.
1066 Recessive MYH6 Mutations in Hypoplastic Left Heart With Reduced Ejection Fraction. Circ
1067 Cardiovasc Genet. 2015;8(4):564-71. doi: 10.1161/CIRCGENETICS.115.001070.
1068 10. Zanon A, Kalvakuri S, Rakovic A, Foco L, Guida M, Schwienbacher C, et al. SLP-2
1069 interacts with Parkin in mitochondria and prevents mitochondrial dysfunction in Parkin-deficient
1070 human iPSC-derived neurons and Drosophila. Hum Mol Genet. 2017;26(13):2412-25. doi:
1071 10.1093/hmg/ddx132. PubMed PMID: 28379402.
1072 11. Dasgupta C, Martinez AM, Zuppan CW, Shah MM, Bailey LL, Fletcher WH.
1073 Identification of connexin43 (alpha1) gap junction gene mutations in patients with hypoplastic left
1074 heart syndrome by denaturing gradient gel electrophoresis (DGGE). Mutat Res. 2001;479(1-
1075 2):173-86. doi: 10.1016/s0027-5107(01)00160-9.
1076 12. Yagi H, Liu X, Gabriel GC, Wu Y, Peterson K, Murray SA, et al. The Genetic Landscape
1077 of Hypoplastic Left Heart Syndrome. Pediatr Cardiol. 2018;39(6):1069-81. doi: 10.1007/s00246-
1078 018-1861-4. PubMed PMID: 29569026.
1079 13. Yaich L, Ooi J, Park M, Borg JP, Landry C, Bodmer R, et al. Functional analysis of the
1080 Numb phosphotyrosine-binding domain using site-directed mutagenesis. The Journal of biological
1081 chemistry. 1998;273(17):10381-8. PubMed PMID: 9553095.
1082 14. Grossfeld P, Ye M, Harvey R. Hypoplastic left heart syndrome: new genetic insights. J Am
1083 Coll Cardiol. 2009;53(12):1072-4. doi: 10.1016/j.jacc.2008.12.024. PubMed PMID: 19298922.

15. Miao Y, Tian L, Martin M, Paige SL, Galdos FX, Li J, et al. Intrinsic Endocardial Defects Contribute to Hypoplastic Left Heart Syndrome. Cell Stem Cell. 2020;27(4):574-89.e8. doi: 10.1016/j.stem.2020.07.015.
16. Liu X, Yagi H, Saeed S, Bais AS, Gabriel GC, Chen Z, et al. The complex genetics of hypoplastic left heart syndrome. Nat Genet. 2017;49(7):1152-9. doi: 10.1038/ng.3870.
17. Gaber N, Gagliardi M, Patel P, Kinnear C, Zhang C, Chitayat D, et al. Fetal reprogramming and senescence in hypoplastic left heart syndrome and in human pluripotent stem cells during cardiac differentiation. Am J Pathol. 2013;183(3):720-34. doi: 10.1016/j.ajpath.2013.05.022.
18. Theis JL, Vogler G, Missinato MA, Li X, Nielsen T, Zeng X-XI, et al. Patient-specific genomics and cross-species functional analysis implicate LRP2 in hypoplastic left heart syndrome. eLife. 2020;9:e59554. doi: 10.7554/eLife.59554.
19. Bodmer R. The gene tinman is required for specification of the heart and visceral muscles in Drosophila. Development. 1993;118(3):719-29.
20. Bodmer R. Heart development in Drosophila and its relationship to vertebrates. Trends in Cardiovascular Medicine. 1995;5(1):21-8. doi: 10.1016/1050-1738(94)00032-Q.
21. Cripps RM, Olson EN. Control of cardiac development by an evolutionarily conserved transcriptional network. Dev Biol. 2002;246(1):14-28. doi: 10.1006/dbio.2002.0666.
22. Bodmer R, Frasch M. Chapter 1.2 - Development and Aging of the Drosophila Heart. In: Rosenthal N, Harvey RP, editors. Heart Development and Regeneration. Boston: Academic Press; 2010. p. 47-86.
23. Bier E, Bodmer R. Drosophila, an emerging model for cardiac disease. Gene. 2004;342(1):1-11. doi: 10.1016/j.gene.2004.07.018.
24. Evans SM, Yelon D, Conlon FL, Kirby ML. Myocardial lineage development. Circ Res. 2010;107(12):1428-44. doi: 10.1161/CIRCRESAHA.110.227405.
25. Bakkers J. Zebrafish as a model to study cardiac development and human cardiac disease. Cardiovasc Res. 2011;91(2):279-88. doi: 10.1093/cvr/cvr098.
26. Liu J, Stainier DYR. Zebrafish in the study of early cardiac development. Circ Res. 2012;110(6):870-4. doi: 10.1161/CIRCRESAHA.111.246504.
27. Fink M, Callol-Massot C, Chu A, Ruiz-Lozano P, Izpisua Belmonte JC, Giles W, et al. A new method for detection and quantification of heartbeat parameters in Drosophila, zebrafish, and embryonic mouse hearts. Biotechniques. 2009;46(2):101-13. doi: 10.2144/000113078.
28. Huang G-Y, Xie L-J, Linask KL, Zhang C, Zhao X-Q, Yang Y, et al. Evaluating the role of connexin43 in congenital heart disease: Screening for mutations in patients with outflow tract anomalies and the analysis of knock-in mouse models. J Cardiovasc Dis Res. 2011;2(4):206-12. doi: 10.4103/0975-3583.89804.
29. Yu MS, Spiering S, Colas AR. Generation of First Heart Field-like Cardiac Progenitors and Ventricular-like Cardiomyocytes from Human Pluripotent Stem Cells. JoVE (Journal of Visualized Experiments). 2018;(136):e57688. doi: 10.3791/57688.
30. Paige SL, Galdos FX, Lee S, Chin ET, Ranjbarvaziri S, Feyen DAM, et al. Patient-Specific Induced Pluripotent Stem Cells Implicate Intrinsic Impaired Contractility in Hypoplastic Left Heart Syndrome. Circulation. 2020;142(16):1605-8. doi: 10.1161/CIRCULATIONAHA.119.045317.
31. Diez-Cunado M, Wei K, Bushway PJ, Maurya MR, Perera R, Subramaniam S, et al. miRNAs that Induce Human Cardiomyocyte Proliferation Converge on the Hippo Pathway. Cell reports. 2018;23(7):2168-74. Epub 2018/05/17. doi: 10.1016/j.celrep.2018.04.049. PubMed PMID: 29768213; PubMed Central PMCID: PMCPMC6261450.

1130 32. Murphy SA, Miyamoto M, Kervadec A, Kannan S, Tampakakis E, Kambhampati S, et al.
1131 PGC1/PPAR drive cardiomyocyte maturation at single cell level via YAP1 and SF3B2. Nature
1132 communications. 2021;12(1):1648. Epub 2021/03/14. doi: 10.1038/s41467-021-21957-z. PubMed
1133 PMID: 33712605; PubMed Central PMCID: PMCPMC7955035.
1134 33. Cunningham TJ, Yu MS, McKeithan WL, Spiering S, Carrette F, Huang C-T, et al. Id
1135 genes are essential for early heart formation. Genes Dev. 2017;31(13):1325-38. doi:
1136 10.1101/gad.300400.117.
1137 34. Cunningham TJ, Yu MS, McKeithan WL, Spiering S, Carrette F, Huang CT, et al. Id genes
1138 are essential for early heart formation. Genes & development. 2017. doi: 10.1101/gad.300400.117.
1139 PubMed PMID: 28794185.
1140 35. Zhang Z, Li M, Wang H, Agrawal S, Zhang R. Antisense therapy targeting MDM2
1141 oncogene in prostate cancer: Effects on proliferation, apoptosis, multiple gene expression, and
1142 chemotherapy. Proc Natl Acad Sci U S A. 2003;100(20):11636-41. Epub 2003/09/18. doi:
1143 10.1073/pnas.1934692100. PubMed PMID: 13130078; PubMed Central PMCID:
1144 PMCPMC208810.
1145 36. Yuan LL, Green A, David L, Dozier C, Recher C, Didier C, et al. Targeting CHK1 inhibits
1146 cell proliferation in FLT3-ITD positive acute myeloid leukemia. Leuk Res. 2014;38(11):1342-9.
1147 Epub 2014/10/05. doi: 10.1016/j.leukres.2014.08.020. PubMed PMID: 25281057.
1148 37. Zhou X, Liao WJ, Liao JM, Liao P, Lu H. Ribosomal proteins: functions beyond the
1149 ribosome. J Mol Cell Biol. 2015;7(2):92-104. Epub 2015/03/05. doi: 10.1093/jmcb/mjv014.
1150 PubMed PMID: 25735597; PubMed Central PMCID: PMCPMC4481666.
1151 38. Mi H, Muruganujan A, Ebert D, Huang X, Thomas PD. PANTHER version 14: more
1152 genomes, a new PANTHER GO-slim and improvements in enrichment analysis tools. Nucleic
1153 Acids Res. 2019;47(D1):D419-D26. doi: 10.1093/nar/gky1038.
1154 39. Szklarczyk D, Gable AL, Lyon D, Junge A, Wyder S, Huerta-Cepas J, et al. STRING v11:
1155 protein-protein association networks with increased coverage, supporting functional discovery in
1156 genome-wide experimental datasets. Nucleic Acids Res. 2019;47(D1):D607-D13. doi:
1157 10.1093/nar/gky1131.
1158 40. Brand AH, Perrimon N. Targeted gene expression as a means of altering cell fates and
1159 generating dominant phenotypes. Development. 1993;118(2):401-15.
1160 41. Gaber N, Gagliardi M, Patel P, Kinnear C, Zhang C, Chitayat D, et al. Fetal reprogramming
1161 and senescence in hypoplastic left heart syndrome and in human pluripotent stem cells during
1162 cardiac differentiation. Am J Pathol. 2013;183(3):720-34. doi: 10.1016/j.ajpath.2013.05.022.
1163 PubMed PMID: 23871585.
1164 42. Liu X, Yagi H, Saeed S, Bais AS, Gabriel GC, Chen Z, et al. The complex genetics of
1165 hypoplastic left heart syndrome. Nature genetics. 2017;49(7):1152-9. doi: 10.1038/ng.3870.
1166 PubMed PMID: 28530678.
1167 43. Schroeder AM, Allahyari M, Vogler G, Missinato MA, Nielsen T, Yu MS, et al. Model
1168 system identification of novel congenital heart disease gene candidates: focus on RPL13. Hum
1169 Mol Genet. 2019;28(23):3954-69. doi: 10.1093/hmg/ddz213.
1170 44. Fink M, Callol-Massot C, Chu A, Ruiz-Lozano P, Izpisua Belmonte JC, Giles W, et al. A
1171 new method for detection and quantification of heartbeat parameters in Drosophila, zebrafish, and
1172 embryonic mouse hearts. Biotechniques. 2009;46(2):101-13. doi: 10.2144/000113078. PubMed
1173 PMID: 19317655; PubMed Central PMCID: PMC2855226.

45. Uechi T, Nakajima Y, Nakao A, Torihara H, Chakraborty A, Inoue K, et al. Ribosomal Protein Gene Knockdown Causes Developmental Defects in Zebrafish. PLOS ONE. 2006;1(1):e37. doi: 10.1371/journal.pone.0000037.
46. Ikeda F, Yoshida K, Toki T, Uechi T, Ishida S, Nakajima Y, et al. Exome sequencing identified RPS15A as a novel causative gene for Diamond-Blackfan anemia. Haematologica. 2017;102(3):e93-e6. doi: 10.3324/haematol.2016.153932.
47. Miura GI, Yelon D. A Guide to Analysis of Cardiac Phenotypes in the Zebrafish Embryo. Methods Cell Biol. 2011;101:161-80. doi: 10.1016/B978-0-12-387036-0.00007-4.
48. Fischer M. Census and evaluation of p53 target genes. Oncogene. 2017;36(28):3943-56. Epub 2017/03/14. doi: 10.1038/onc.2016.502. PubMed PMID: 28288132; PubMed Central PMCID: PMCPMC5511239.
49. Robu ME, Larson JD, Nasevicius A, Beiraghi S, Brenner C, Farber SA, et al. p53 activation by knockdown technologies. PLoS Genet. 2007;3(5):e78. doi: 10.1371/journal.pgen.0030078.
50. Furth N, Aylon Y, Oren M. p53 shades of Hippo. Cell Death Differ. 2018;25(1):81-92. doi: 10.1038/cdd.2017.163.
51. Baker NE, Kiparaki M, Khan C. A potential link between p53, cell competition and ribosomopathy in mammals and in Drosophila. Dev Biol. 2019;446(1):17-9. doi: 10.1016/j.ydbio.2018.11.018.
52. Ollmann M, Young LM, Di Como CJ, Karim F, Belvin M, Robertson S, et al. Drosophila p53 is a structural and functional homolog of the tumor suppressor p53. Cell. 2000;101(1):91-101. doi: 10.1016/S0092-8674(00)80626-1. PubMed PMID: 10778859.
53. Raj N, Bam R. Reciprocal Crosstalk Between YAP1/Hippo Pathway and the p53 Family Proteins: Mechanisms and Outcomes in Cancer. Front Cell Dev Biol. 2019;7:159. Epub 20190809. doi: 10.3389/fcell.2019.00159. PubMed PMID: 31448276; PubMed Central PMCID: PMCPMC6695833.
54. Monroe TO, Hill MC, Morikawa Y, Leach JP, Heallen T, Cao S, et al. YAP Partially Reprograms Chromatin Accessibility to Directly Induce Adult Cardiogenesis In Vivo. Developmental Cell. 2019;48(6):765-79.e7. doi: 10.1016/j.devcel.2019.01.017.
55. Kang J, Brajanovski N, Chan KT, Xuan J, Pearson RB, Sanij E. Ribosomal proteins and human diseases: molecular mechanisms and targeted therapy. Signal Transduct Target Ther. 2021;6(1):323. Epub 2021/09/01. doi: 10.1038/s41392-021-00728-8. PubMed PMID: 34462428; PubMed Central PMCID: PMCPMC8405630.
56. Bruneau BG, Logan M, Davis N, Levi T, Tabin CJ, Seidman JG, et al. Chamber-specific cardiac expression of Tbx5 and heart defects in Holt-Oram syndrome. Developmental biology. 1999;211(1):100-8. doi: 10.1006/dbio.1999.9298. PubMed PMID: 10373308.
57. Qian L, Wythe JD, Liu J, Cartry J, Vogler G, Mohapatra B, et al. Tinman/Nkx2-5 acts via miR-1 and upstream of Cdc42 to regulate heart function across species. J Cell Biol. 2011;193(7):1181-96. doi: 10.1083/jcb.201006114. PubMed PMID: 21690310; PubMed Central PMCID: PMCPMC3216339.
58. Lee KH, Xu Q, Breitbart RE. A new tinman-related gene, nkx2.7, anticipates the expression of nkx2.5 and nkx2.3 in zebrafish heart and pharyngeal endoderm. Dev Biol. 1996;180(2):722-31. doi: 10.1006/dbio.1996.0341.
59. Targoff KL, Schell T, Yelon D. Nkx Genes Regulate Heart Tube Extension and Exert Differential Effects on Ventricular and Atrial Cell Number. Dev Biol. 2008;322(2):314-21. doi: 10.1016/j.ydbio.2008.07.037.

1219 60. Tiu GC, Kerr CH, Forester CM, Krishnarao PS, Rosenblatt HD, Raj N, et al. A p53-
1220 dependent translational program directs tissue-selective phenotypes in a model of
1221 ribosomopathies. Developmental Cell. 2021;0(0). doi: 10.1016/j.devcel.2021.06.013.
1222 61. McGowan KA, Pang WW, Bhardwaj R, Perez MG, Pluvinage JV, Glader BE, et al.
1223 Reduced ribosomal protein gene dosage and p53 activation in low-risk myelodysplastic syndrome.
1224 Blood. 2011;118(13):3622-33. Epub 20110725. doi: 10.1182/blood-2010-11-318584. PubMed
1225 PMID: 21788341; PubMed Central PMCID: PMCPMC3186336.
1226 62. Flucke U, van Noesel MM, Siozopoulou V, Creytens D, Tops BBJ, van Gorp JM, et al.
1227 EWSR1-The Most Common Rearranged Gene in Soft Tissue Lesions, Which Also Occurs in
1228 Different Bone Lesions: An Updated Review. Diagnostics (Basel). 2021;11(6). Epub 20210615.
1229 doi: 10.3390/diagnostics11061093. PubMed PMID: 34203801; PubMed Central PMCID:
1230 PMCPMC8232650.
1231 63. Vlachos A, Osorio DS, Atsidaftos E, Kang J, Lababidi ML, Seiden HS, et al. The Increased
1232 Prevalence of Congenital Heart Disease (CHD) in Children with Diamond Blackfan Anemia
1233 (DBA) Suggests Unrecognized DBA as a Cause of CHD in the General Population: A Report of
1234 the Diamond Blackfan Anemia Registry. Circ Genom Precis Med. 2018;11(5):e002044. doi:
1235 10.1161/CIRCGENETICS.117.002044.
1236 64. Jin SC, Homsy J, Zaidi S, Lu Q, Morton S, DePalma SR, et al. Contribution of rare
1237 inherited and de novo variants in 2,871 congenital heart disease probands. Nat Genet.
1238 2017;49(11):1593-601. doi: 10.1038/ng.3970.
1239 65. Ye M, Coldren C, Liang X, Mattina T, Goldmuntz E, Benson DW, et al. Deletion of ETS-
1240 1, a gene in the Jacobsen syndrome critical region, causes ventricular septal defects and abnormal
1241 ventricular morphology in mice. Hum Mol Genet. 2010;19(4):648-56. Epub 20091126. doi:
1242 10.1093/hmg/ddp532. PubMed PMID: 19942620; PubMed Central PMCID: PMCPMC2807373.
1243 66. Kathiriya IS, Rao KS, Iacono G, Devine WP, Blair AP, Hota SK, et al. Modeling Human
1244 TBX5 Haploinsufficiency Predicts Regulatory Networks for Congenital Heart Disease.
1245 Developmental cell. 2021;56(3):292-309 e9. Epub 2020/12/16. doi:
1246 10.1016/j.devcel.2020.11.020. PubMed PMID: 33321106; PubMed Central PMCID:
1247 PMCPMC7878434.
1248 67. Ang YS, Rivas RN, Ribeiro AJS, Srivas R, Rivera J, Stone NR, et al. Disease Model of
1249 GATA4 Mutation Reveals Transcription Factor Cooperativity in Human Cardiogenesis. Cell.
1250 2016;167(7):1734-49 e22. doi: 10.1016/j.cell.2016.11.033. PubMed PMID: 27984724; PubMed
1251 Central PMCID: PMCPMC5180611.
1252 68. Tanaka M, Yamaguchi S, Yamazaki Y, Kinoshita H, Kuwahara K, Nakao K, et al. Somatic
1253 chromosomal translocation between Ewsr1 and Fli1 loci leads to dilated cardiomyopathy in a
1254 mouse model. Sci Rep. 2015;5:7826. Epub 20150116. doi: 10.1038/srep07826. PubMed PMID:
1255 25591392; PubMed Central PMCID: PMCPMC5379005.
1256 69. Ragni CV, Diguet N, Le Garrec JF, Novotova M, Resende TP, Pop S, et al. Amotl1
1257 mediates sequestration of the Hippo effector Yap1 downstream of Fat4 to restrict heart growth.
1258 Nat Commun. 2017;8:14582. Epub 20170227. doi: 10.1038/ncomms14582. PubMed PMID:
1259 28239148; PubMed Central PMCID: PMCPMC5333361.
1260 70. Danilova N, Gazda HT. Ribosomopathies: how a common root can cause a tree of
1261 pathologies. Dis Model Mech. 2015;8(9):1013-26. doi: 10.1242/dmm.020529.
1262 71. Boulon S, Westman BJ, Hutten S, Boisvert F-M, Lamond AI. The nucleolus under stress.
1263 Mol Cell. 2010;40(2):216-27. doi: 10.1016/j.molcel.2010.09.024.

1264 72. Yang K, Yang J, Yi J. Nucleolar Stress: hallmarks, sensing mechanism and diseases. Cell
1265 Stress. 2018;2(6):125-40. doi: 10.15698/cst2018.06.139.
1266 73. Dai M-S, Zeng SX, Jin Y, Sun X-X, David L, Lu H. Ribosomal protein L23 activates p53
1267 by inhibiting MDM2 function in response to ribosomal perturbation but not to translation
1268 inhibition. Mol Cell Biol. 2004;24(17):7654-68. doi: 10.1128/MCB.24.17.7654-7668.2004.
1269 74. Zhang Y, Lu H. Signaling to p53: ribosomal proteins find their way. Cancer Cell.
1270 2009;16(5):369-77. doi: 10.1016/j.ccr.2009.09.024.
1271 75. Men H, Cai H, Cheng Q, Zhou W, Wang X, Huang S, et al. The regulatory roles of p53 in
1272 cardiovascular health and disease. Cell Mol Life Sci. 2021;78(5):2001-18. Epub 20201111. doi:
1273 10.1007/s00018-020-03694-6. PubMed PMID: 33179140.
1274 76. Mak TW, Hauck L, Grothe D, Billia F. p53 regulates the cardiac transcriptome. Proc Natl
1275 Acad Sci U S A. 2017;114(9):2331-6. Epub 20170213. doi: 10.1073/pnas.1621436114. PubMed
1276 PMID: 28193895; PubMed Central PMCID: PMCPMC5338492.
1277 77. Deisenroth C, Zhang Y. The Ribosomal Protein-Mdm2-p53 Pathway and Energy
1278 Metabolism. Genes Cancer. 2011;2(4):392-403. doi: 10.1177/1947601911409737.
1279 78. Liu Y, Deisenroth C, Zhang Y. RP–MDM2–p53 Pathway: Linking Ribosomal Biogenesis
1280 and Tumor Surveillance. Trends Cancer. 2016;2(4):191-204. doi: 10.1016/j.trecan.2016.03.002.
1281 79. Cui Z, DiMario PJ. RNAi knockdown of Nopp140 induces Minute-like phenotypes in
1282 Drosophila. Mol Biol Cell. 2007;18(6):2179-91. doi: 10.1091/mbc.e07-01-0074.
1283 80. Barron DA, Kagey JD. The role of the Hippo pathway in human disease and tumorigenesis.
1284 Clin Transl Med. 2014;3:25. doi: 10.1186/2001-1326-3-25.
1285 81. Del Re DP. The hippo signaling pathway: implications for heart regeneration and disease.
1286 Clin Transl Med. 2014;3(1):27. doi: 10.1186/s40169-014-0027-0.
1287 82. Yu L, Daniels JP, Wu H, Wolf MJ. Cardiac hypertrophy induced by active Raf depends on
1288 Yorkie-mediated transcription. Sci Signal. 2015;8(362):ra13-ra. doi: 10.1126/scisignal.2005719.
1289 83. Wang J, Liu S, Heallen T, Martin JF. The Hippo pathway in the heart: pivotal roles in
1290 development, disease, and regeneration. Nat Rev Cardiol. 2018;15(11):672-84. doi:
1291 10.1038/s41569-018-0063-3.
1292 84. Xiao Y, Leach J, Wang J, Martin JF. Hippo/Yap Signaling in Cardiac Development and
1293 Regeneration. Curr Treat Options Cardiovasc Med. 2016;18(6):38. doi: 10.1007/s11936-016-
1294 0461-y.
1295 85. von Gise A, Lin Z, Schlegelmilch K, Honor LB, Pan GM, Buck JN, et al. YAP1, the nuclear
1296 target of Hippo signaling, stimulates heart growth through cardiomyocyte proliferation but not
1297 hypertrophy. Proceedings of the National Academy of Sciences of the United States of America.
1298 2012;109(7):2394-9. doi: 10.1073/pnas.1116136109.
1299 86. Del Re DP, Yang Y, Nakano N, Cho J, Zhai P, Yamamoto T, et al. Yes-associated protein
1300 isoform 1 (Yap1) promotes cardiomyocyte survival and growth to protect against myocardial
1301 ischemic injury. J Biol Chem. 2013;288(6):3977-88. doi: 10.1074/jbc.M112.436311.
1302 87. Gifford CA, Ranade SS, Samarakoon R, Salunga HT, de Soysa TY, Huang Y, et al.
1303 Oligogenic inheritance of a human heart disease involving a genetic modifier. Science.
1304 2019;364(6443):865-70. Epub 20190530. doi: 10.1126/science.aat5056. PubMed PMID:
1305 31147515; PubMed Central PMCID: PMCPMC6557373.
1306 88. Birla AK, Brimmer S, Short WD, Olutoye OO, 2nd, Shar JA, Lalwani S, et al. Current state
1307 of the art in hypoplastic left heart syndrome. Front Cardiovasc Med. 2022;9:878266. Epub
1308 20221028. doi: 10.3389/fcvm.2022.878266. PubMed PMID: 36386362; PubMed Central PMCID:
1309 PMCPMC9651920.

1310 89. Theis JL, Vogler G, Missinato MA, Li X, Nielsen T, Zeng XI, et al. Patient-specific
1311 genomics and cross-species functional analysis implicate LRP2 in hypoplastic left heart syndrome.
1312 eLife. 2020;9. Epub 2020/10/03. doi: 10.7554/eLife.59554. PubMed PMID: 33006316; PubMed
1313 Central PMCID: PMCPMC7581429.
1314 90. Miao Y, Tian L, Martin M, Paige SL, Galdos FX, Li J, et al. Intrinsic Endocardial Defects
1315 Contribute to Hypoplastic Left Heart Syndrome. Cell stem cell. 2020;27(4):574-89 e8. Epub
1316 20200817. doi: 10.1016/j.stem.2020.07.015. PubMed PMID: 32810435; PubMed Central PMCID:
1317 PMCPMC7541479.
1318 91. Xu X, Jin K, Bais AS, Zhu W, Yagi H, Feinstein TN, et al. Uncompensated mitochondrial
1319 oxidative stress underlies heart failure in an iPSC-derived model of congenital heart disease. Cell
1320 stem cell. 2022;29(5):840-55 e7. Epub 20220407. doi: 10.1016/j.stem.2022.03.003. PubMed
1321 PMID: 35395180; PubMed Central PMCID: PMCPMC9302582.
1322 92. Bray MA, Singh S, Han H, Davis CT, Borgeson B, Hartland C, et al. Cell Painting, a high-
1323 content image-based assay for morphological profiling using multiplexed fluorescent dyes. Nature
1324 protocols. 2016;11(9):1757-74. Epub 20160825. doi: 10.1038/nprot.2016.105. PubMed PMID:
1325 27560178; PubMed Central PMCID: PMCPMC5223290.
1326 93. Karczewski KJ, Francioli LC, Tiao G, Cummings BB, Alföldi J, Wang Q, et al. The
1327 mutational constraint spectrum quantified from variation in 141,456 humans. Nature.
1328 2020;581(7809):434-43. doi: 10.1038/s41586-020-2308-7.
1329 94. Grodecká L, Kramárek M, Lockerová P, Kováčová T, Ravčuková B, Richterová R, et al.
1330 No major effect of the CDH1 c.2440-6C>G mutation on splicing detected in last exon-specific
1331 splicing minigene assay. Genes, Chromosomes and Cancer. 2014;53(9):798-801. doi:
1332 https://doi.org/10.1002/gcc.22186.
1333 95. Burridge PW, Holmström A, Wu JC. Chemically Defined Culture and Cardiomyocyte
1334 Differentiation of Human Pluripotent Stem Cells. Curr Protoc Hum Genet. 2015;87:21.3.1-.3.15.
1335 doi: 10.1002/0471142905.hg2103s87.
1336 96. Pei F, Jiang J, Bai S, Cao H, Tian L, Zhao Y, et al. Chemical-defined and albumin-free
1337 generation of human atrial and ventricular myocytes from human pluripotent stem cells. Stem Cell
1338 Research. 2017;19:94-103. doi: 10.1016/j.scr.2017.01.006.
1339 97. Ewels PA, Peltzer A, Fillinger S, Patel H, Alneberg J, Wilm A, et al. The nf-core
1340 framework for community-curated bioinformatics pipelines. Nat Biotechnol. 2020;38(3):276-8.
1341 doi: 10.1038/s41587-020-0439-x. PubMed PMID: 32055031.
1342 98. Love MI, Huber W, Anders S. Moderated estimation of fold change and dispersion for
1343 RNA-seq data with DESeq2. Genome Biol. 2014;15(12):550. doi: 10.1186/s13059-014-0550-8.
1344 PubMed PMID: 25516281; PubMed Central PMCID: PMCPMC4302049.
1345 99. Raudvere U, Kolberg L, Kuzmin I, Arak T, Adler P, Peterson H, et al. g:Profiler: a web
1346 server for functional enrichment analysis and conversions of gene lists (2019 update). Nucleic
1347 Acids Res. 2019;47(W1):W191-W8. doi: 10.1093/nar/gkz369. PubMed PMID: 31066453;
1348 PubMed Central PMCID: PMCPMC6602461.
1349 100. Hu Y, Flockhart I, Vinayagam A, Bergwitz C, Berger B, Perrimon N, et al. An integrative
1350 approach to ortholog prediction for disease-focused and other functional studies. BMC
1351 Bioinformatics. 2011;12:357. doi: 10.1186/1471-2105-12-357. PubMed PMID: 21880147;
1352 PubMed Central PMCID: PMCPMC3179972.
1353 101. Han Z, Yi P, Li X, Olson EN. Hand, an evolutionarily conserved bHLH transcription factor
1354 required for Drosophila cardiogenesis and hematopoiesis. Development. 2006;133(6):1175-82.
1355 doi: 10.1242/dev.02285.

1356 102. Tögel M, Meyer H, Lehmacher C, Heinisch JJ, Pass G, Paululat A. The bHLH transcription
1357 factor hand is required for proper wing heart formation in Drosophila. Dev Biol. 2013;381(2):446-
1358 59. doi: 10.1016/j.ydbio.2013.05.027.
1359 103. Hallier B, Hoffmann J, Roeder T, Tögel M, Meyer H, Paululat A. The bHLH Transcription
1360 Factor Hand Regulates the Expression of Genes Critical to Heart and Muscle Function in
1361 Drosophila melanogaster. PLOS ONE. 2015;10(8):e0134204. doi: 10.1371/journal.pone.0134204.
1362 104. Vogler G. gvogler/FlyHearts-tdtK-Rscripts: First release of the R tdtK script. First ed:
1363 Zenodo; 2021.
1364 105. Cammarato A, Ocorr S, Ocorr K. Enhanced assessment of contractile dynamics in
1365 Drosophila hearts. BioTechniques. 2015;58(2):77-80. doi: 10.2144/000114255. PubMed PMID:
1366 25652030.
1367 106. Alayari NN, Vogler G, Taghli-Lamallem O, Ocorr K, Bodmer R, Cammarato A.
1368 Fluorescent labeling of Drosophila heart structures. J Vis Exp. 2009;(32). doi: 10.3791/1423.
1369 107. Ocorr K, Vogler G, Bodmer R. Methods to assess Drosophila heart development, function
1370 and aging. Methods. 2014;68(1):265-72. doi: 10.1016/j.ymeth.2014.03.031.
1371 108. Huang C-J, Tu C-T, Hsiao C-D, Hsieh F-J, Tsai H-J. Germ-line transmission of a
1372 myocardium-specific GFP transgene reveals critical regulatory elements in the cardiac myosin
1373 light chain 2 promoter of zebrafish. Dev Dyn. 2003;228(1):30-40. doi: 10.1002/dvdy.10356.
1374 109. Schumacher JA, Bloomekatz J, Garavito-Aguilar ZV, Yelon D. tal1 Regulates the
1375 formation of intercellular junctions and the maintenance of identity in the endocardium. Dev Biol.
1376 2013;383(2):214-26. doi: 10.1016/j.ydbio.2013.09.019.
1377 110. Westerfield M. The zebrafish book: A guide for the laboratory use of zebrafish
1378 (Brachydanio rerio). 1993 ed: M. W, editor: University of Oregon Press; 1993.
1379 111. Talbot JC, Amacher SL. A streamlined CRISPR pipeline to reliably generate zebrafish
1380 frameshifting alleles. Zebrafish. 2014;11(6):583-5. doi: 10.1089/zeb.2014.1047.
1381 112. Gagnon JA, Valen E, Thyme SB, Huang P, Akhmetova L, Ahkmetova L, et al. Efficient
1382 mutagenesis by Cas9 protein-mediated oligonucleotide insertion and large-scale assessment of
1383 single-guide RNAs. PLOS ONE. 2014;9(5):e98186. doi: 10.1371/journal.pone.0098186.
1384 113. Irion U, Krauss J, Nüsslein-Volhard C. Precise and efficient genome editing in zebrafish
1385 using the CRISPR/Cas9 system. Development. 2014;141(24):4827-30. doi: 10.1242/dev.115584.
1386 114. Ocorr K, Fink M, Cammarato A, Bernstein SI, Bodmer R. Semi-automated Optical
1387 Heartbeat Analysis of Small Hearts. Journal of Visualized Experiments : JoVE. 2009;(31). doi:
1388 10.3791/1435.
1389 115. Zeng X-XI, Yelon D. Cadm4 restricts the production of cardiac outflow tract progenitor
1390 cells. Cell Reports. 2014;7(4):951-60. doi: 10.1016/j.celrep.2014.04.013.
1391 116. Pradhan A, Zeng X-XI, Sidhwani P, Marques SR, George V, Targoff KL, et al. FGF
1392 signaling enforces cardiac chamber identity in the developing ventricle. Development.
1393 2017;144(7):1328-38. doi: 10.1242/dev.143719.
1394 117. Alexander J, Stainier DY, Yelon D. Screening mosaic F1 females for mutations affecting
1395 zebrafish heart induction and patterning. Dev Genet. 1998;22(3):288-99. doi: 10.1002/(SICI)1520-
1396 6408(1998)22:3<288::AID-DVG10>3.0.CO;2-2.
1397 118. Hoshijima K, Jurynec MJ, Klatt Shaw D, Jacobi AM, Behlke MA, Grunwald DJ. Highly
1398 Efficient CRISPR-Cas9-Based Methods for Generating Deletion Mutations and F0 Embryos that
1399 Lack Gene Function in Zebrafish. Developmental Cell. 2019;51(5):645-57.e4. doi:
1400 10.1016/j.devcel.2019.10.004.
1401

Figure 1

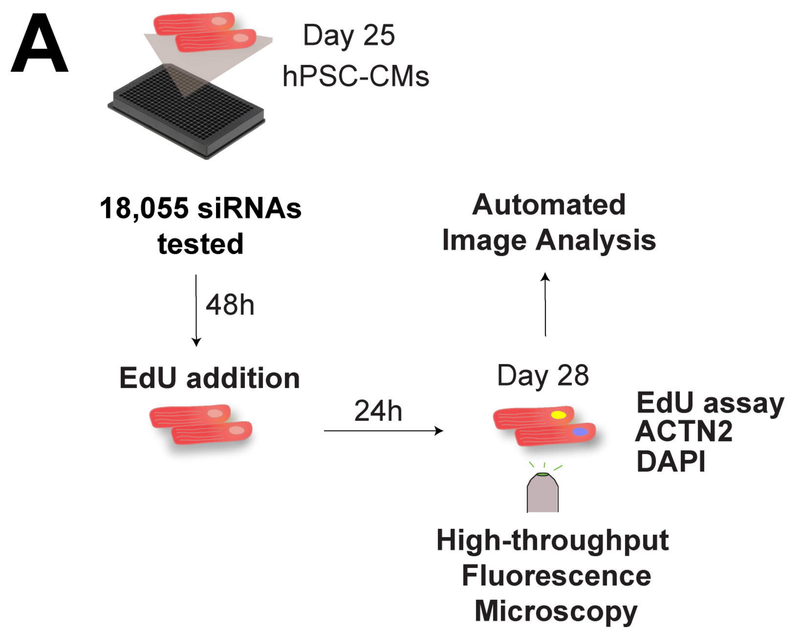

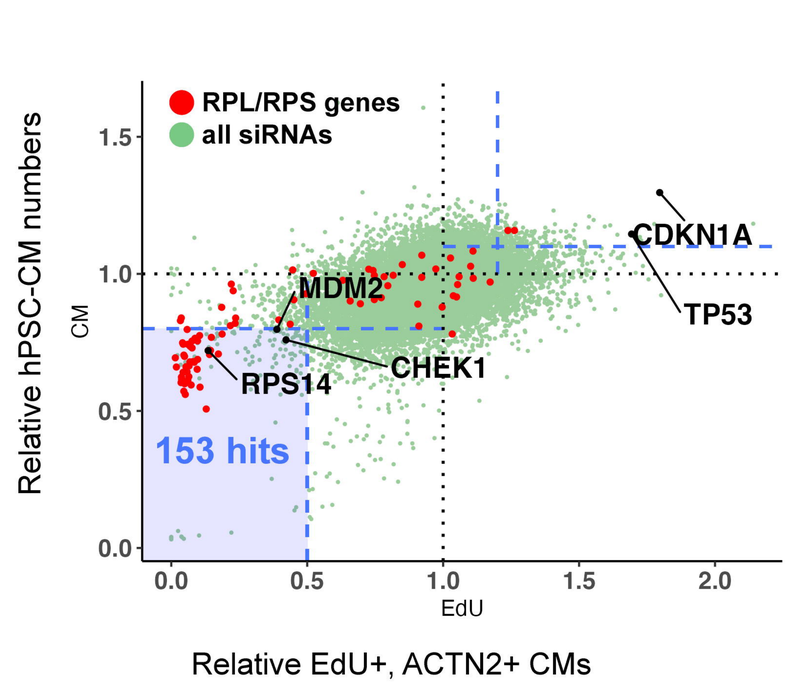

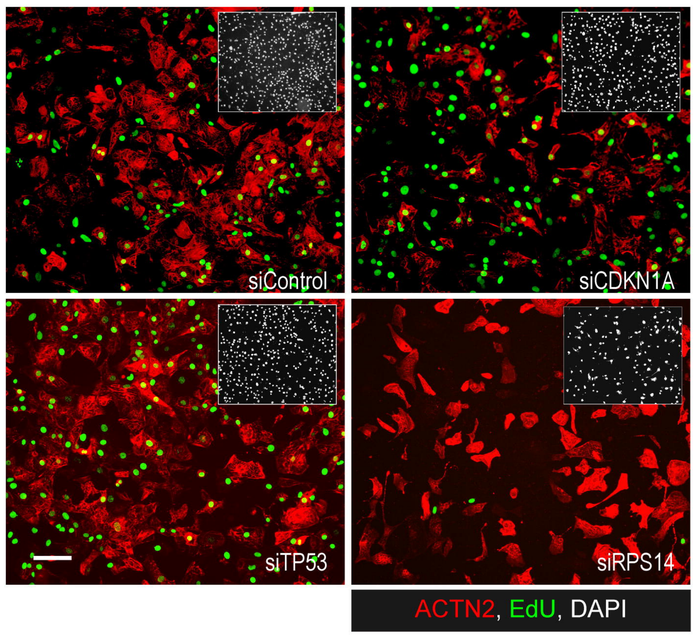

D Enrichment of 153 top hits (Biological Process, BP)

Term	P value	Genes
nuclear-transcribed mRNA catabolic process	1.94e-43	41
protein targeting to ER	3.17e-56	41
establishment of protein localization to organelle	9.35e-30	43
Ribosome	1.78e-46	42
signal transduction by p53 class mediator	4.87e-02	8
positive regulation of vascular endothelial growth factor signaling pathway	3.20e-02	2
regulation of intrinsic apoptotic signaling pathway by p53 class mediator	3.73e-02	3
regulation of signal transduction by p53 class mediator	6.05e-03	8
ribosomal small subunit assembly	2.09e-07	6
ribosomal large subunit assembly	2.03e-06	6
negative regulation of smoothened signaling pathway	4.71e-02	3

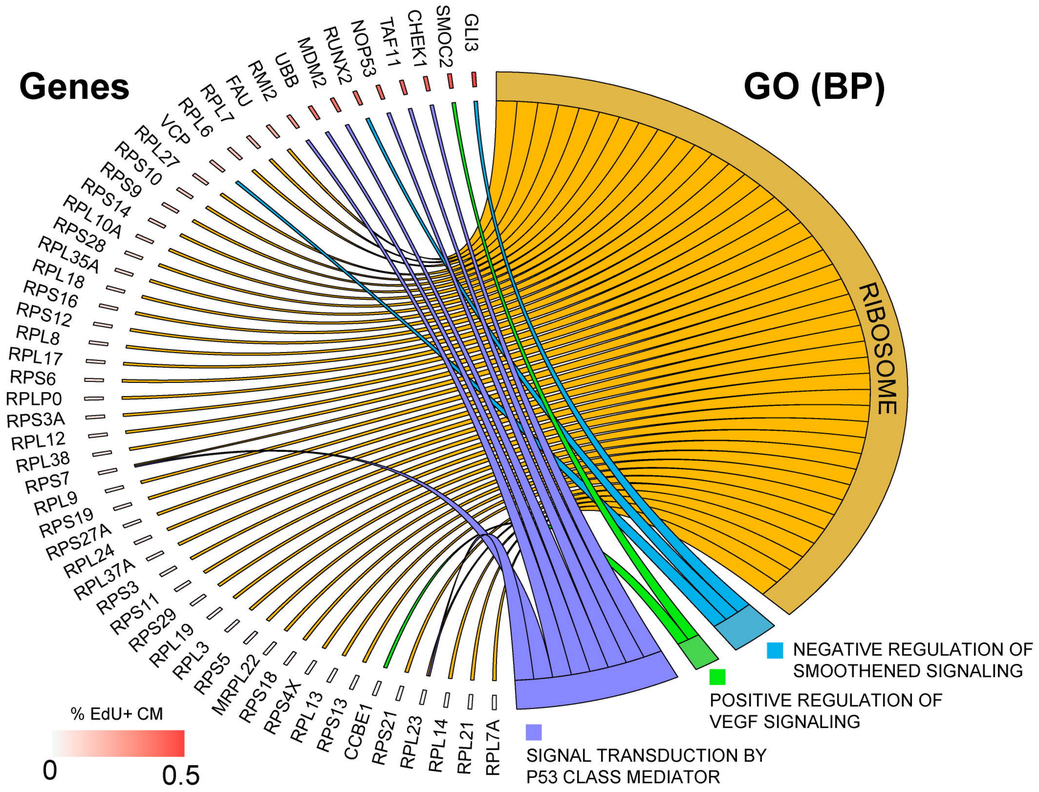

Figure 2

A

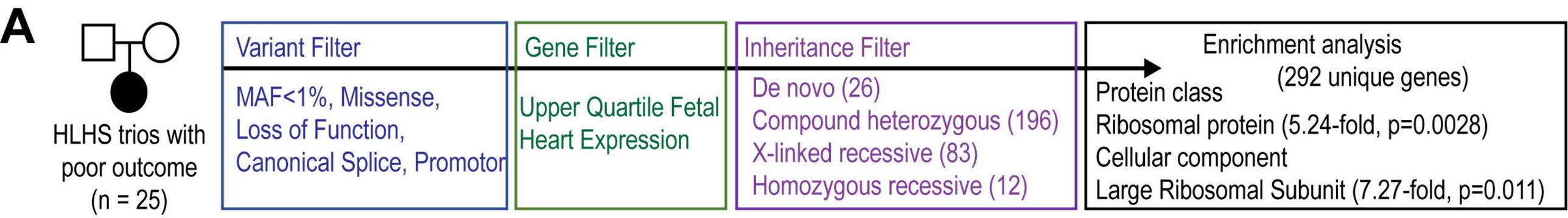

B

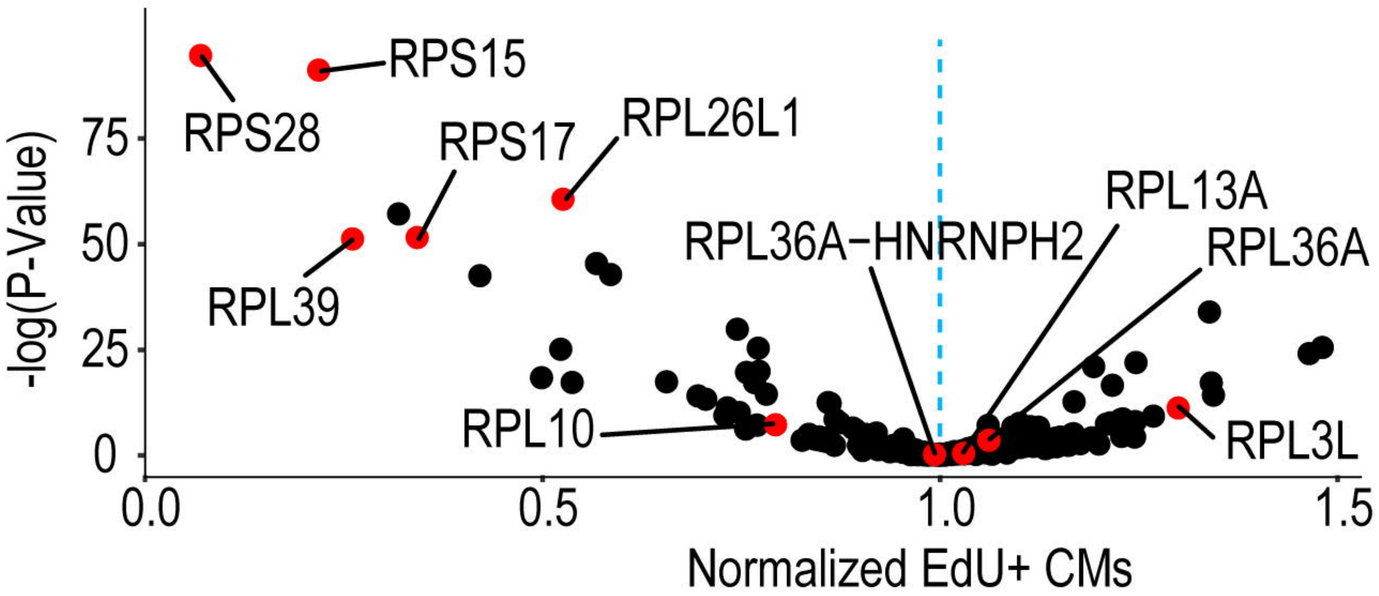

C

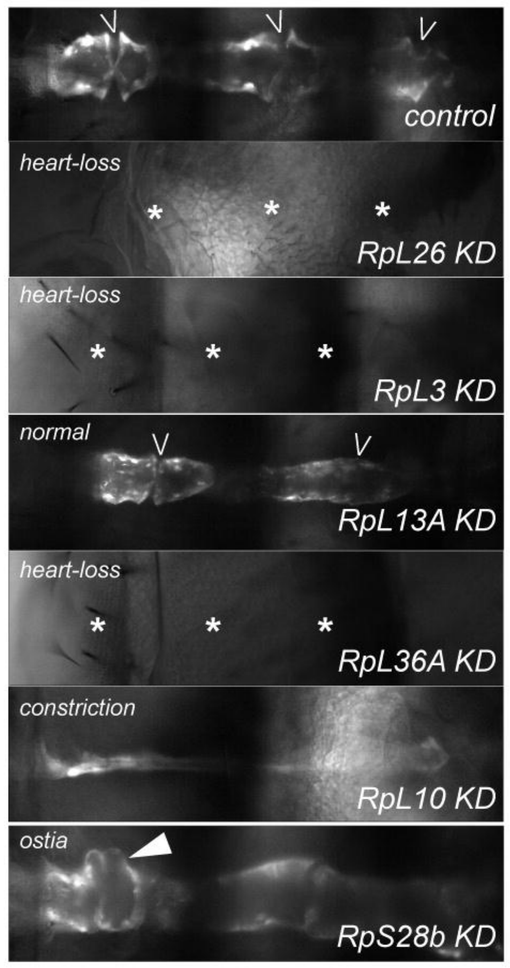

Hand 4.2-Gal4; R94C02::tdTom x RNAi

D

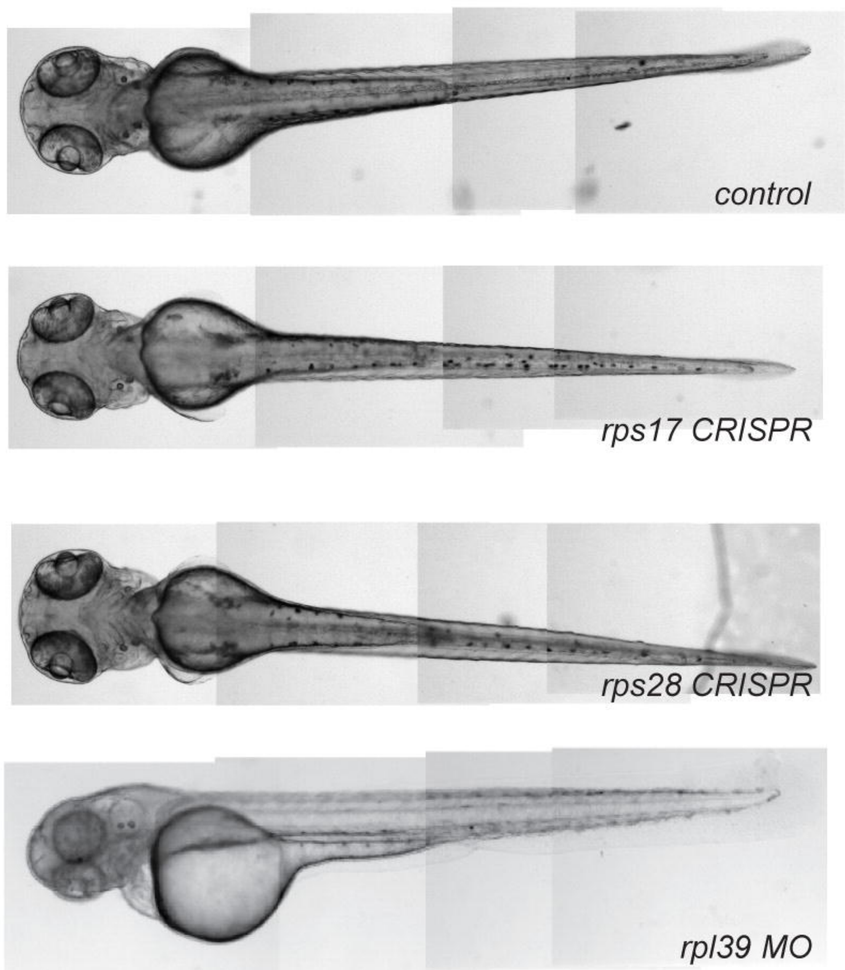

72 hpf

E

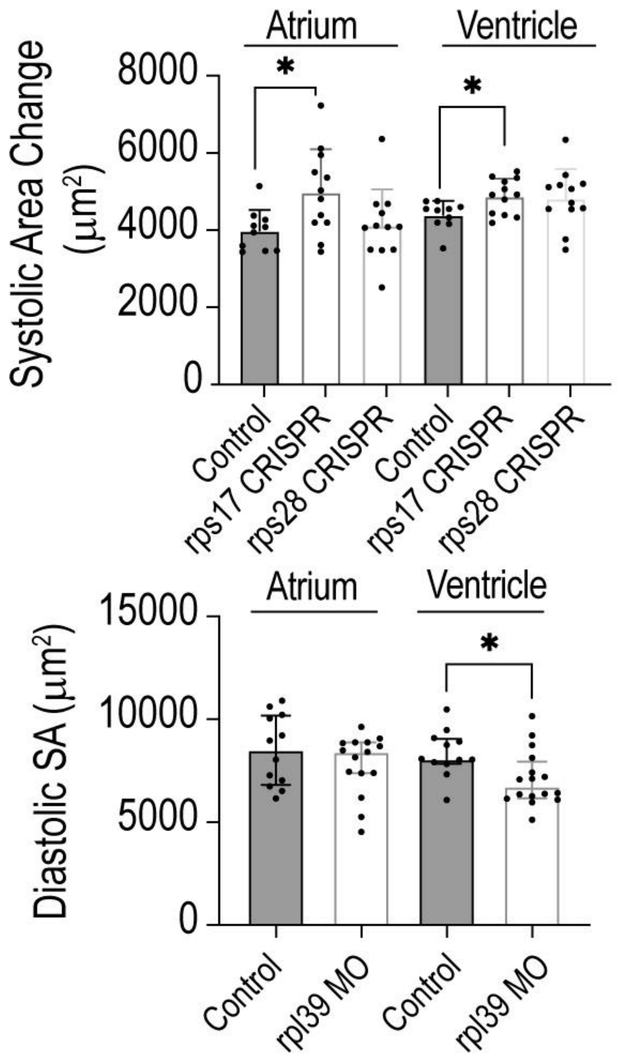

Figure 3

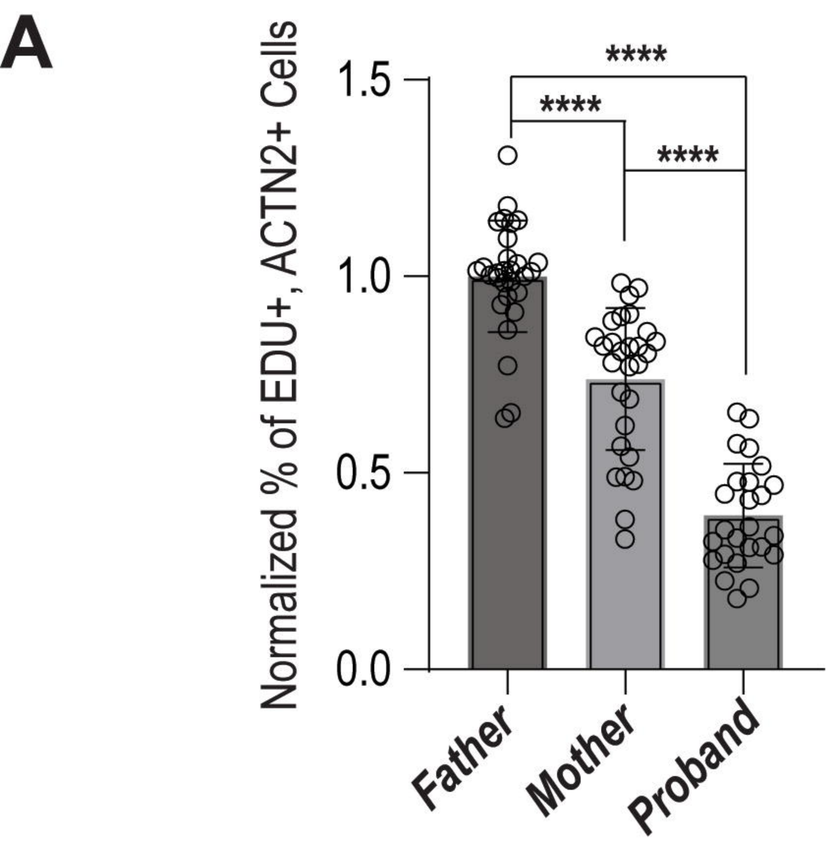
A
Normalized % of EDU+, ACTN2+ Cells
1.5
1.0
0.5
0.0
****
****
****
Father
Mother
Proband

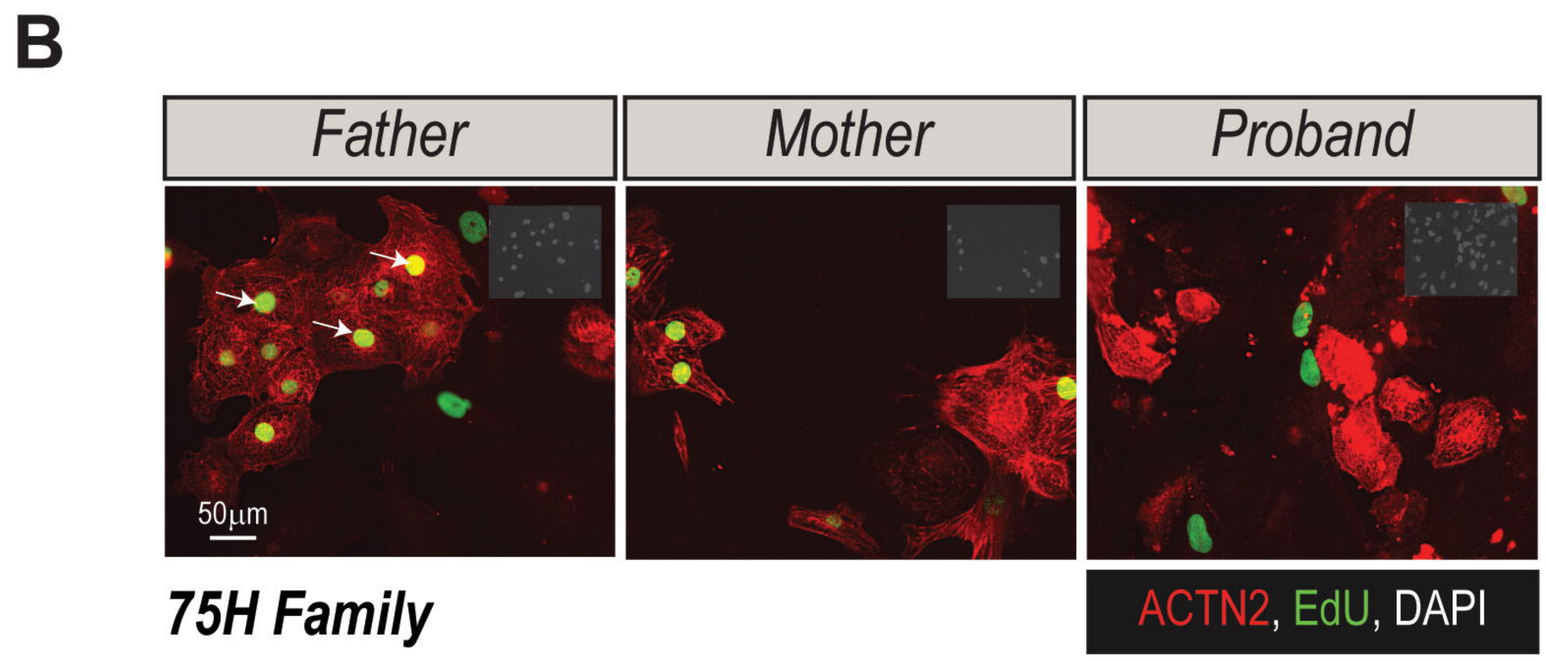
B
Father
Mother
Proband
50µm
75H Family
ACTN2, EdU, DAPI

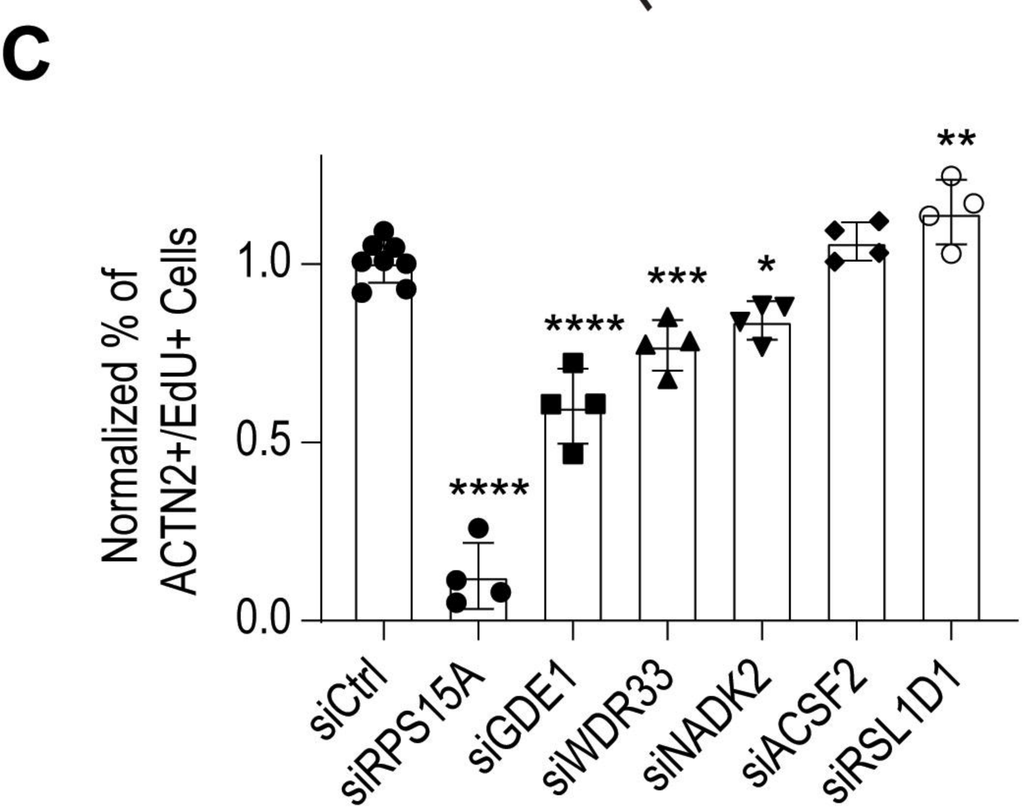
C
Normalized % of ACTN2+/EdU+ Cells
1.0
0.5
0.0
****
****
***
*
**
siCtrl
siRPS15A
siGDE1
siWDR33
siNADK2
siACSF2
siRSL1D1

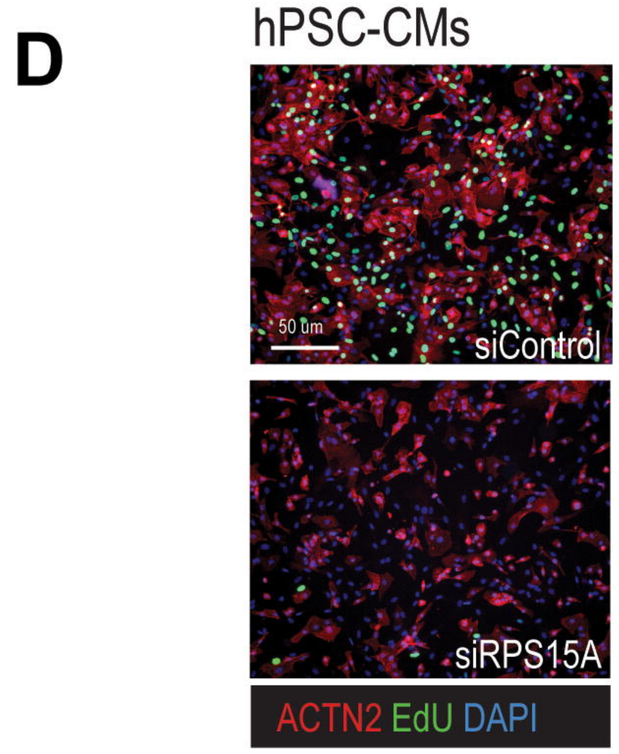
D
hPSC-CMs
50 um
siControl
siRPS15A
ACTN2 EdU DAPI

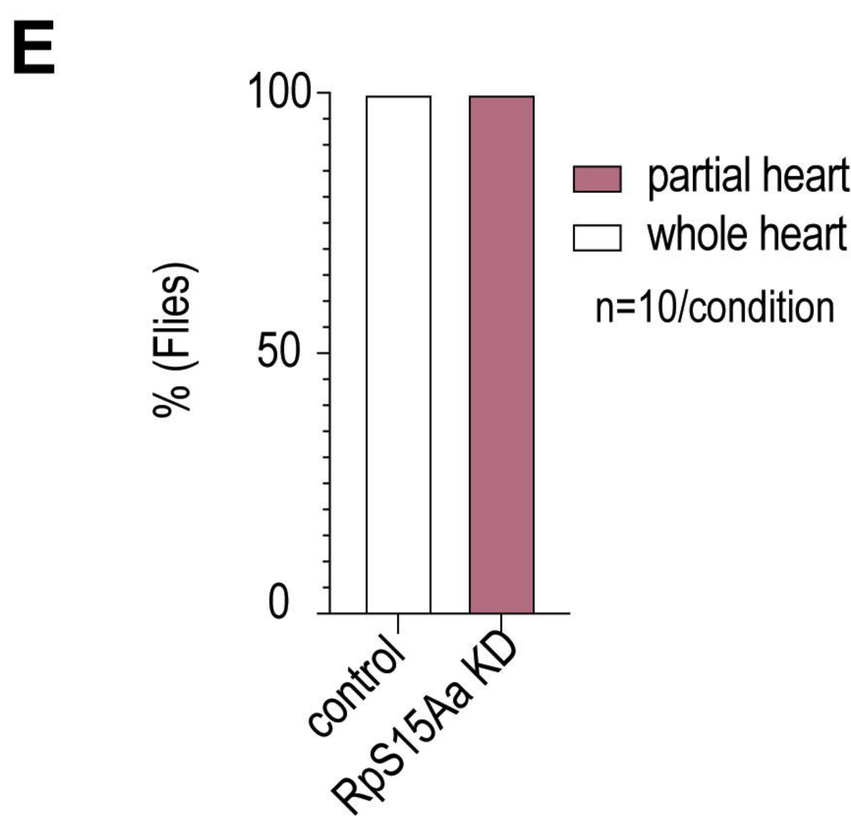
E
100
50
0
% (Flies)
partial heart
whole heart
n=10/condition
control
RpS15Aa KD

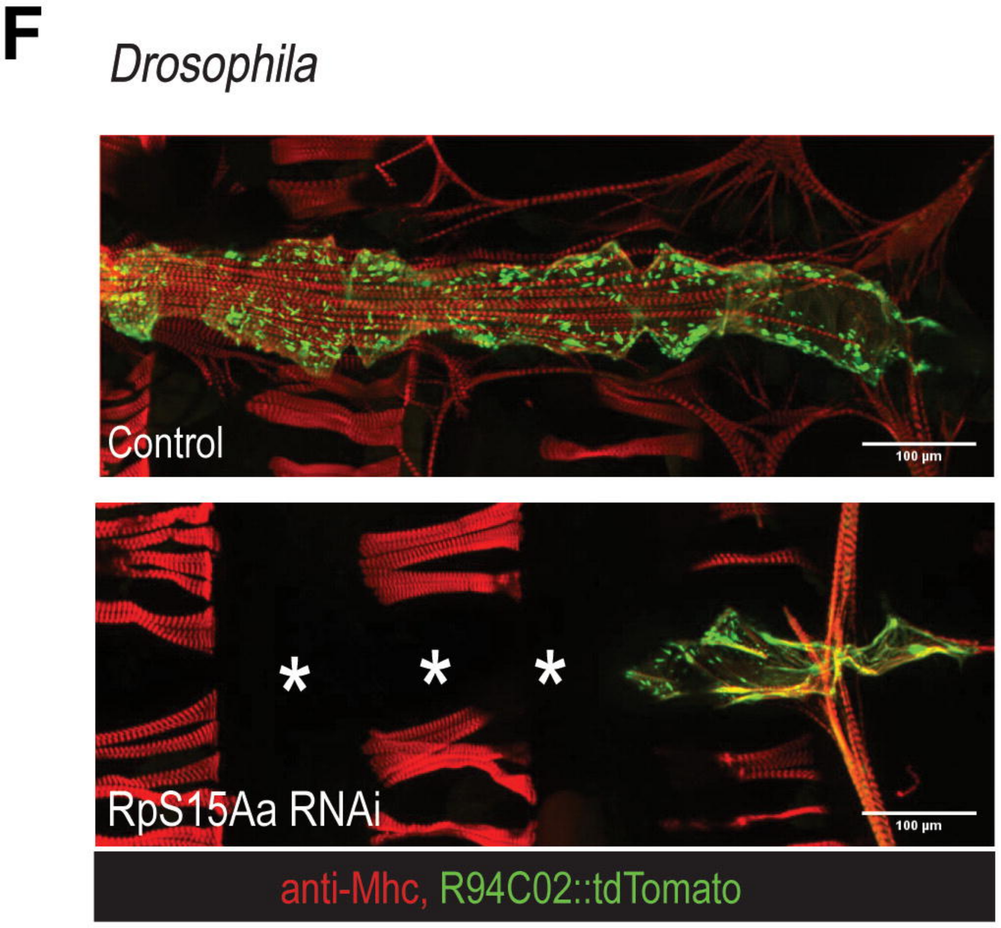
F
Drosophila
Control
100 µm
RpS15Aa RNAi
100 µm
anti-Mhc, R94C02::tdTomato

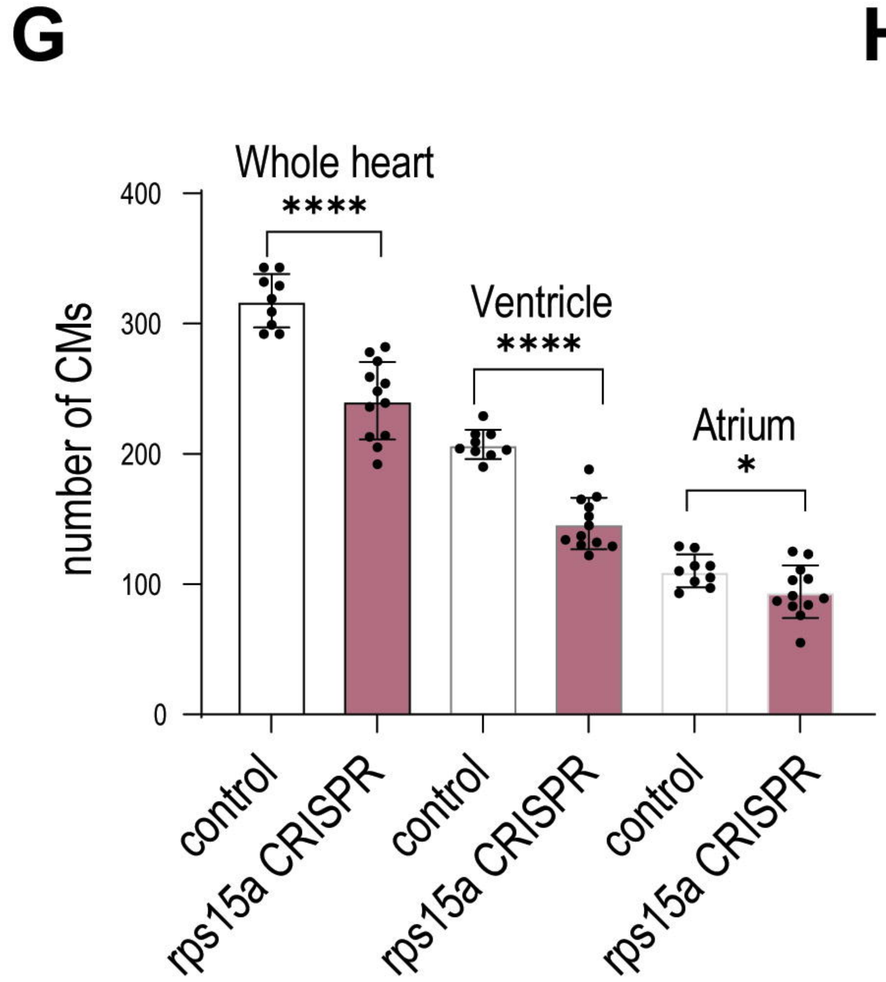
G
Whole heart
****
Ventricle
****
Atrium
*
number of CMs
400
300
200
100
0
control
rps15a CRISPR
control
rps15a CRISPR
control
rps15a CRISPR

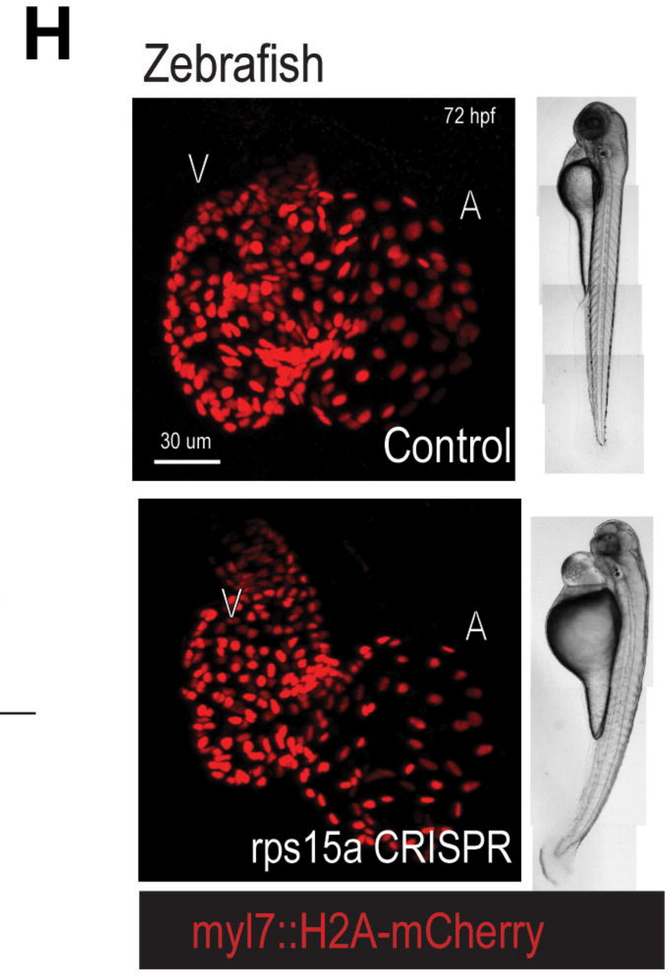
H
Zebrafish
72 hpf
V
A
30 um
Control
V
A
rps15a CRISPR
myl7::H2A-mCherry

Figure 4

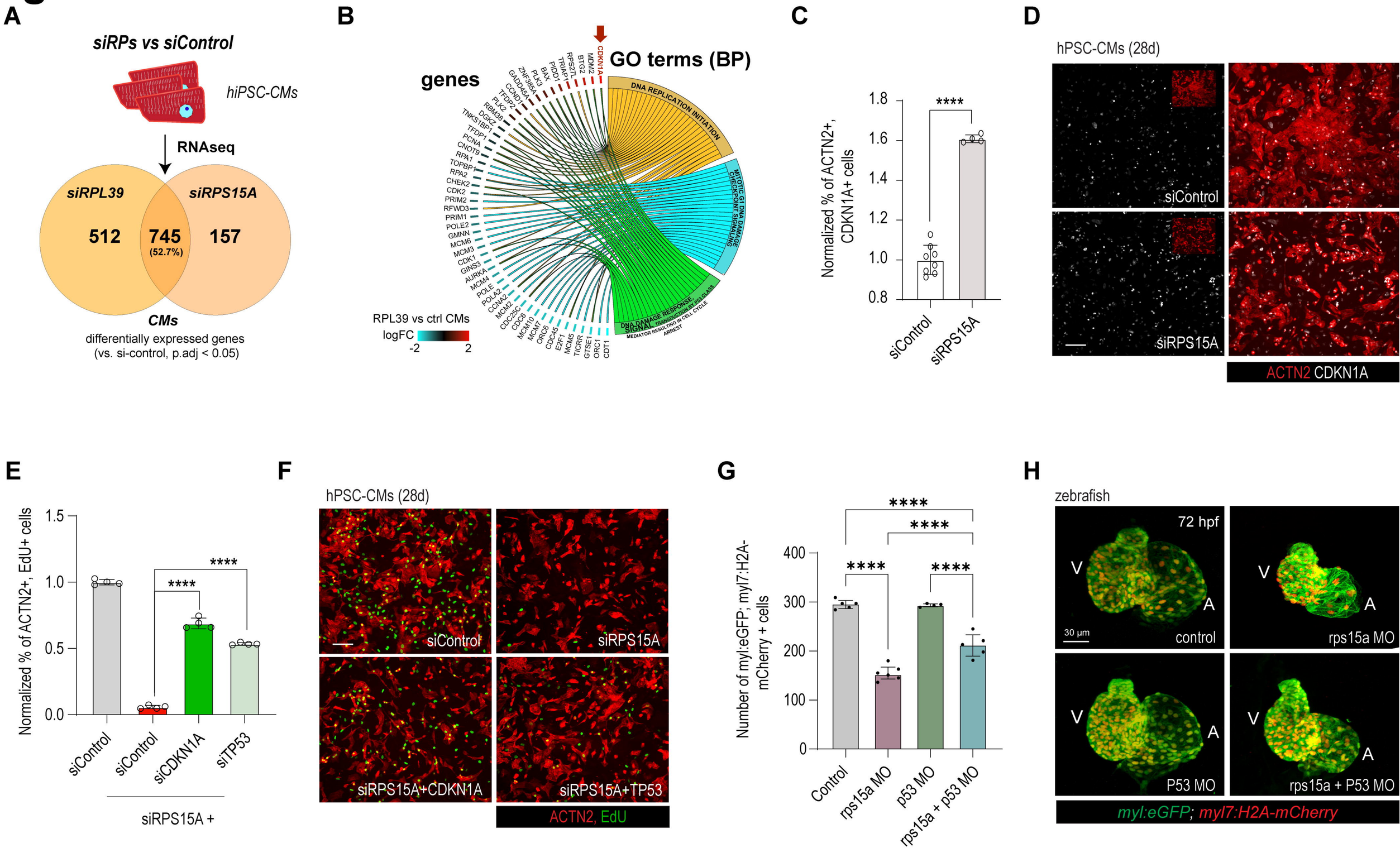
A
siRPs vs siControl
hiPSC-CMs
RNAseq
siRPL39
siRPS15A
512
745
(52.7%)
157
CMs
differentially expressed genes
(vs. si-control, p.adj < 0.05)
B
genes
GO terms (BP)
DNA REPLICATION INITIATION
MITOTIC G1 DNA DAMAGE CHECKPOINT SIGNALING
DNA DAMAGE RESPONSE SIGNAL TRANSDUCTION BY P53 CLASS MEDIATOR RESULTING IN CELL CYCLE ARREST
RPL39 vs ctrl CMs
logFC
-2
2
C
Normalized % of ACTN2+, CDKN1A+ cells
****
siControl
siRPS15A
D
hPSC-CMs (28d)
siControl
siRPS15A
ACTN2 CDKN1A
E
Normalized % of ACTN2+, EdU+ cells
****
****
siControl
siControl
siCDKN1A
siTP53
siRPS15A +
F
hPSC-CMs (28d)
siControl
siRPS15A
siRPS15A+CDKN1A
siRPS15A+TP53
ACTN2, EdU
G
Number of myl:eGFP; myl7:H2A-mCherry + cells
****
****
****
****
Control
rps15a MO
p53 MO
rps15a + p53 MO
H
zebrafish
72 hpf
V
A
30 µm
control
rps15a MO
P53 MO
rps15a + P53 MO
myl:eGFP; myl7:H2A-mCherry

Figure 5

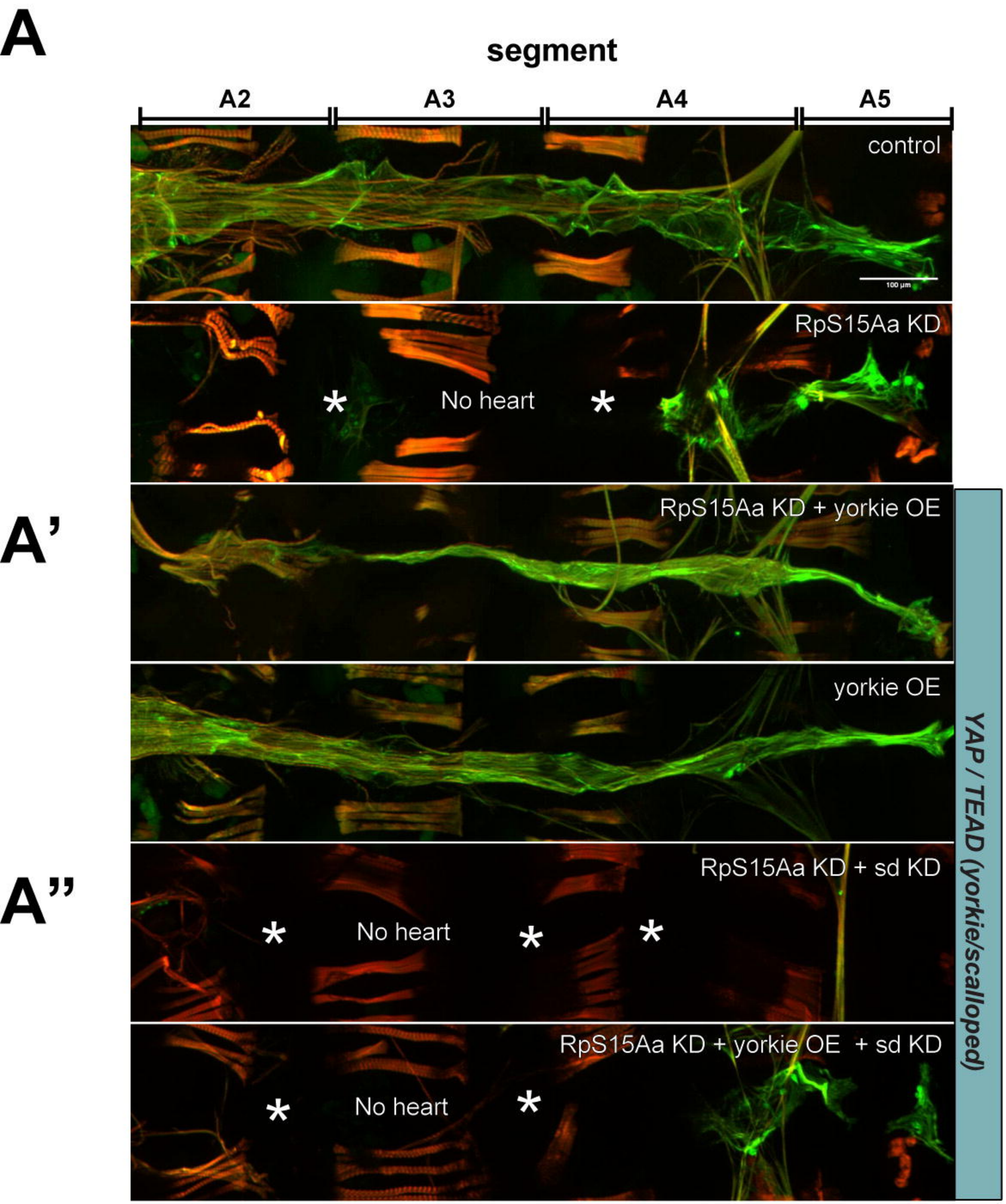
A
segment
A2
A3
A4
A5
control
100 µm
RpS15Aa KD
No heart
A'
RpS15Aa KD + yorkie OE
yorkie OE
A''
RpS15Aa KD + sd KD
No heart
RpS15Aa KD + yorkie OE + sd KD
No heart
YAP / TEAD (yorkie/scalloped)

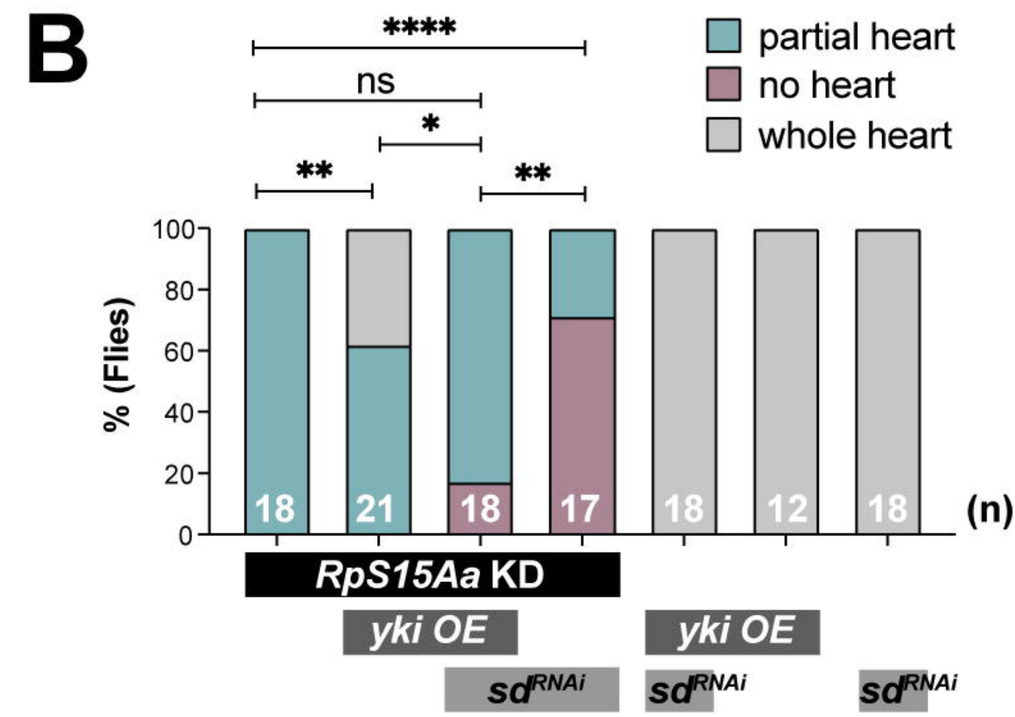
B
****
ns
*
**
**
partial heart
no heart
whole heart
% (Flies)
100
80
60
40
20
0
18
21
18
17
18
12
18
(n)
RpS15Aa KD
yki OE
yki OE
sdRNAi
sdRNAi
sdRNAi

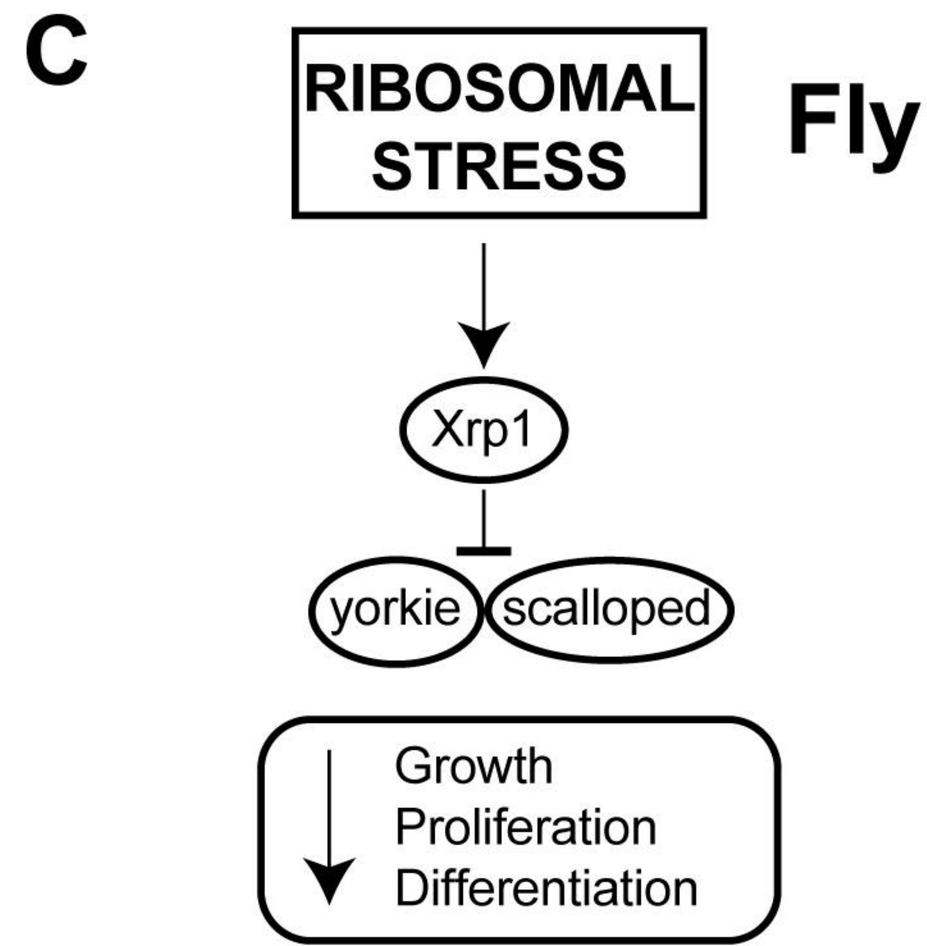
C
RIBOSOMAL STRESS
Fly
Xrp1
yorkie
scalloped
Growth
Proliferation
Differentiation

Figure 6

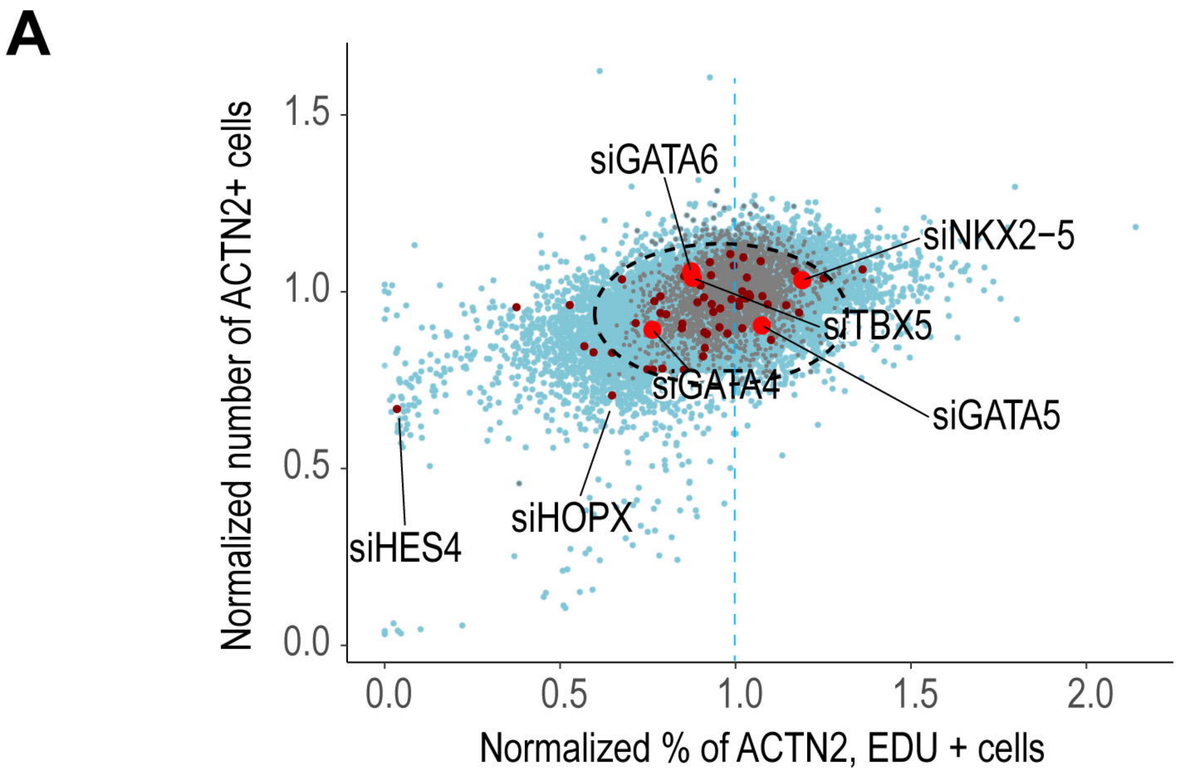
A
Normalized number of ACTN2+ cells
Normalized % of ACTN2, EDU + cells
siGATA6
siNKX2-5
siTBX5
siGATA4
siGATA5
siHOPX
siHES4

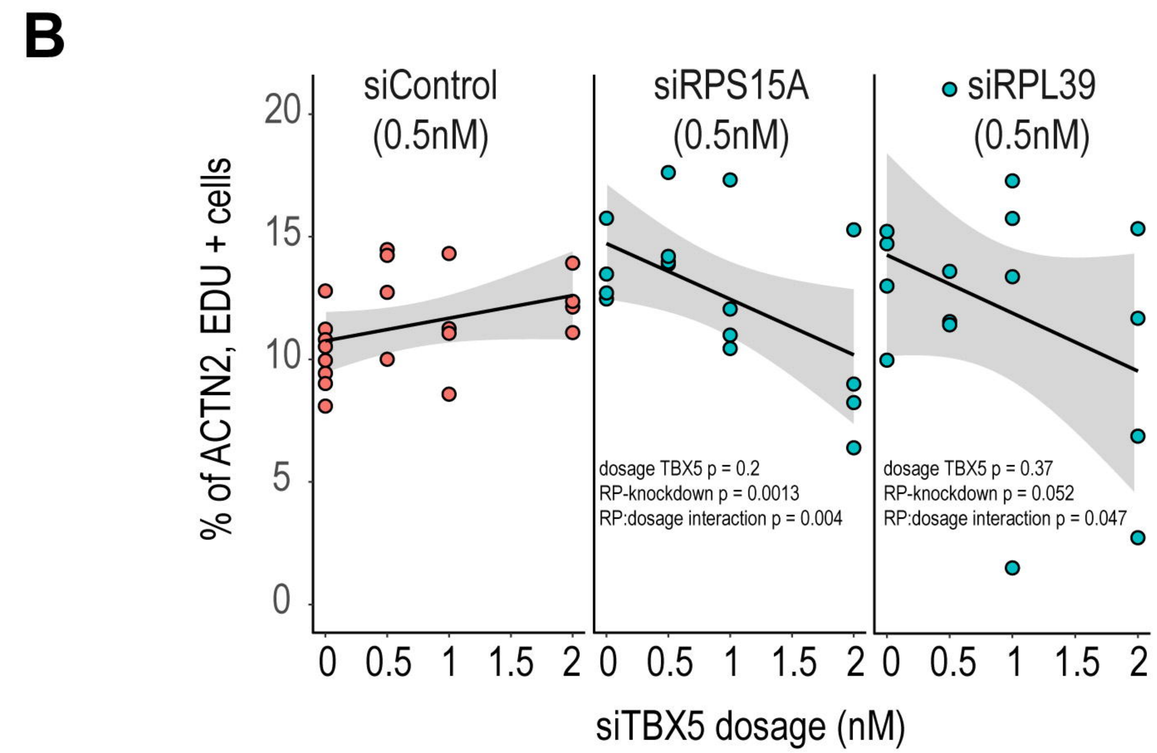
B
siControl (0.5nM)
siRPS15A (0.5nM)
siRPL39 (0.5nM)
% of ACTN2, EDU + cells
dosage TBX5 p = 0.2
RP-knockdown p = 0.0013
RP:dosage interaction p = 0.004
dosage TBX5 p = 0.37
RP-knockdown p = 0.052
RP:dosage interaction p = 0.047
siTBX5 dosage (nM)

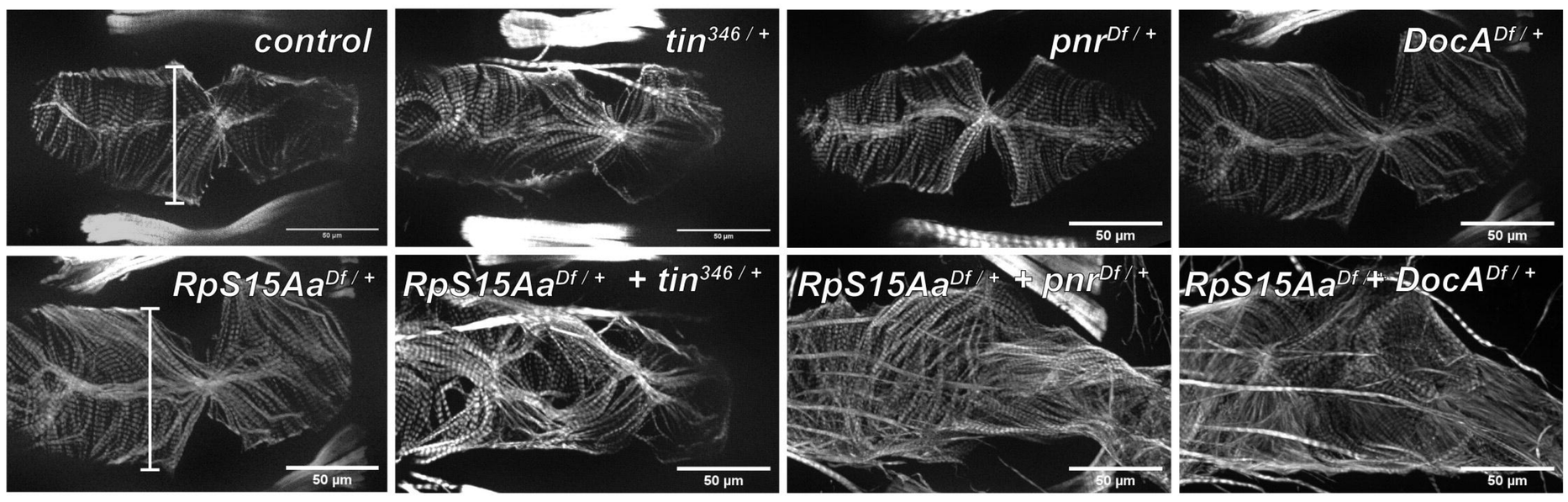
C
control
tin346/+
pnrDf/+
DocADf/+
RpS15AaDf/+
RpS15AaDf/+ + tin346/+
RpS15AaDf/+ + pnrDf/+
RpS15AaDf/+ + DocADf/+
50 µm

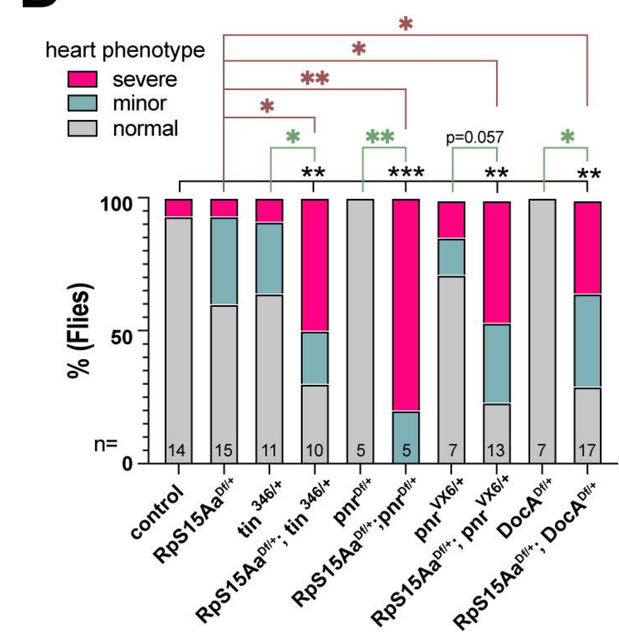
D
heart phenotype
severe
minor
normal
p=0.057
% (Flies)
n=
14 15 11 10 5 5 7 13 7 17
control
RpS15Aa Df/+
tin 346/+
RpS15Aa Df/+; tin 346/+
pnr Df/+
RpS15Aa Df/+; pnr Df/+
pnr VX6/+
RpS15Aa Df/+; pnr VX6/+
DocA Df/+
RpS15Aa Df/+; DocA Df/+

Figure 7

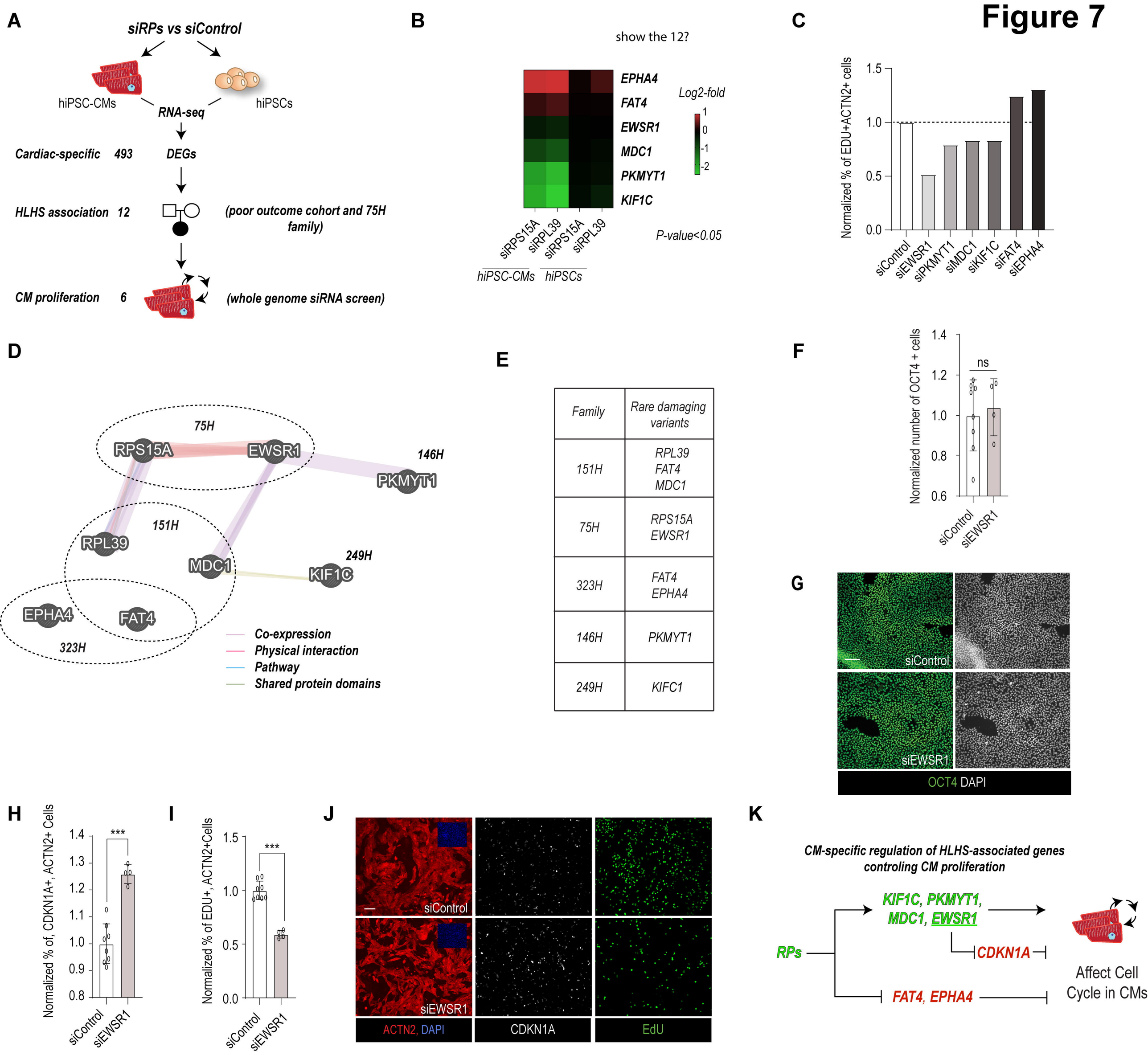
A
siRPs vs siControl
hiPSC-CMs
hiPSCs
RNA-seq
Cardiac-specific 493 DEGs
HLHS association 12
(poor outcome cohort and 75H family)
CM proliferation 6
(whole genome siRNA screen)
B
show the 12?
EPHA4
FAT4
EWSR1
MDC1
PKMYT1
KIF1C
Log2-fold
1
0
-1
-2
siRPS15A
siRPL39
siRPS15A
siRPL39
hiPSC-CMs
hiPSCs
P-value<0.05
C
Normalized % of EDU+ACTN2+ cells
1.5
1.0
0.5
0.0
siControl
siEWSR1
siPKMYT1
siMDC1
siKIF1C
siFAT4
siEPHA4
D
75H
RPS15A
EWSR1
146H
PKMYT1
151H
RPL39
MDC1
249H
KIF1C
EPHA4
FAT4
323H
Co-expression
Physical interaction
Pathway
Shared protein domains
E
Family
Rare damaging variants
151H
RPL39
FAT4
MDC1
75H
RPS15A
EWSR1
323H
FAT4
EPHA4
146H
PKMYT1
249H
KIFC1
F
Normalized number of OCT4 + cells
1.4
1.2
1.0
0.8
0.6
ns
siControl
siEWSR1
G
siControl
siEWSR1
OCT4 DAPI
H
Normalized % of, CDKN1A+, ACTN2+ Cells
1.4
1.3
1.2
1.1
1.0
0.9
0.8
***
siControl
siEWSR1
I
Normalized % of EDU+, ACTN2+Cells
1.5
1.0
0.5
0.0
***
siControl
siEWSR1
J
siControl
siEWSR1
ACTN2, DAPI
CDKN1A
EdU
K
CM-specific regulation of HLHS-associated genes controling CM proliferation
KIF1C, PKMYT1, MDC1, EWSR1
RPs
CDKN1A
FAT4, EPHA4
Affect Cell Cycle in CMs

Figure 8

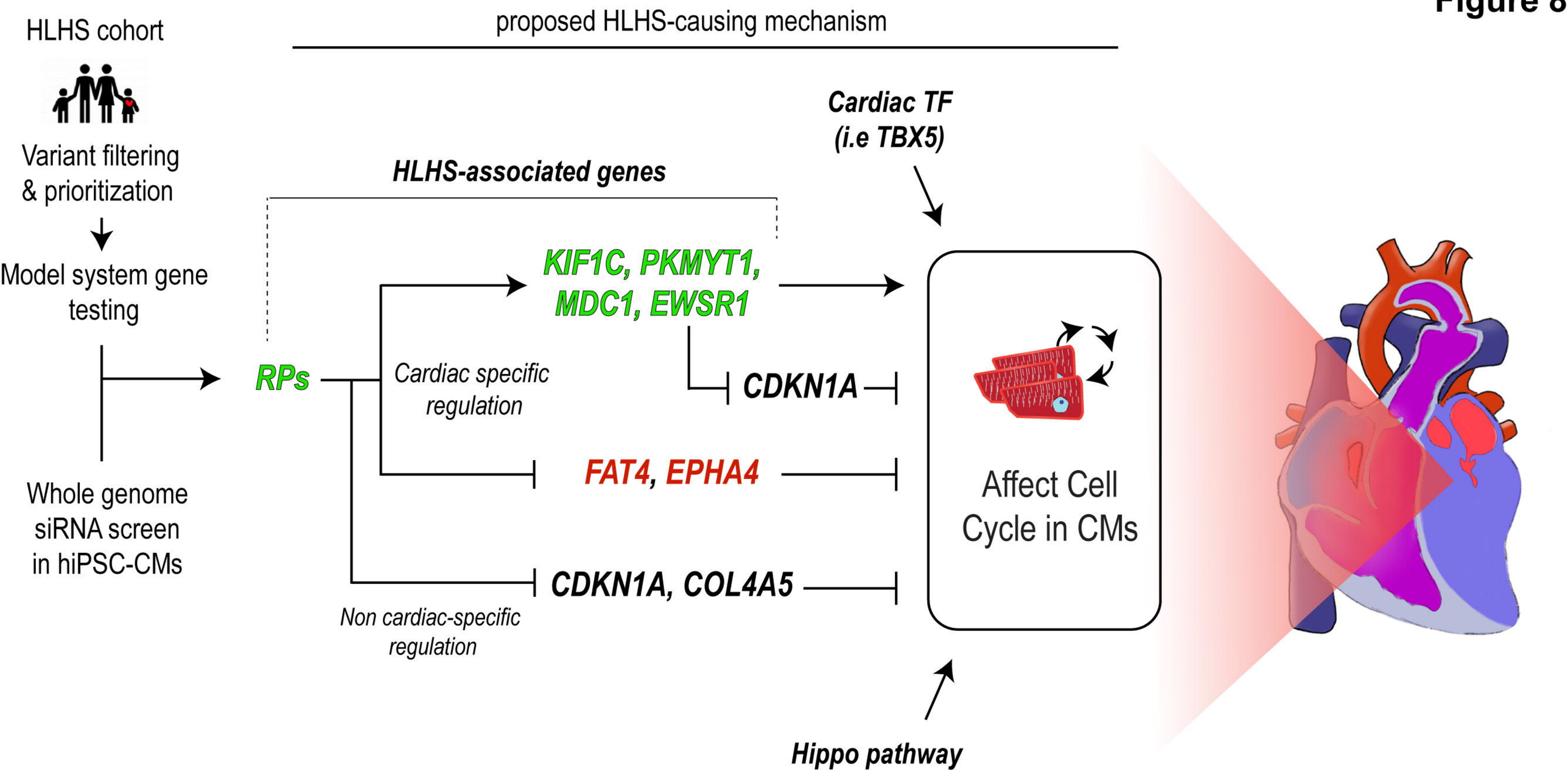
proposed HLHS-causing mechanism
HLHS cohort
Variant filtering & prioritization
Model system gene testing
Whole genome siRNA screen in hiPSC-CMs
HLHS-associated genes
RPs
Cardiac specific regulation
Non cardiac-specific regulation
KIF1C, PKMYT1, MDC1, EWSR1
CDKN1A
FAT4, EPHA4
CDKN1A, COL4A5
Cardiac TF (i.e TBX5)
Hippo pathway
Affect Cell Cycle in CMs